

A COMPREHENSIVE STUDY OF BINARY COMPACT OBJECTS AS GRAVITATIONAL WAVE SOURCES: EVOLUTIONARY CHANNELS, RATES, AND PHYSICAL PROPERTIES

KRZYSZTOF BELCZYNSKI^{1,2,3,4}, VASSILIKI KALOGERA^{1,2} AND TOMASZ BULIK³

¹ Northwestern University, Dept. of Physics & Astronomy, 2145 Sheridan Rd., Evanston, IL 60208

² Harvard-Smithsonian Center for Astrophysics, 60 Garden St., Cambridge, MA 02138;

³ Nicolaus Copernicus Astronomical Center, Bartycka 18, 00-716 Warszawa, Poland;

⁴ Lindheimer Postdoctoral Fellow

belczynski, vicky@northwestern.edu, bulik@camk.edu.pl

Draft version October 22, 2018

ABSTRACT

A new generation of ground-based interferometric detectors for gravitational waves is currently under construction or has entered the commissioning phase (LIGO, VIRGO, GEO600, TAMA). The purpose of these detectors is to observe gravitational waves from astrophysical sources and help improve our understanding of the source origin and physical properties. In this paper we study the most promising candidate sources for these detectors: inspiraling double compact objects. We use population synthesis methods to calculate the properties and coalescence rates of compact object binaries: double neutron stars, black hole-neutron star systems and double black holes. We also examine the formation channels available to double compact object binaries. We explicitly account for the evolution of low-mass helium stars and investigate the possibility of common-envelope evolution involving helium stars as well as two evolved stars. As a result we identify a significant number of new formation channels for double neutron stars, in particular, leading to populations with very distinct properties. We discuss the theoretical and observational implications of such populations, but we also note the need for hydrodynamical calculations to settle the question of whether such common-envelope evolution is possible. We also present and discuss the physical properties of compact object binaries and identify a number of robust, qualitative features as well as their origin. Using the calculated coalescence rates we compare our results to earlier studies and derive expected detection rates for the Laser Interferometer Gravitational-wave Observatory (LIGO). We find that our most optimistic estimate for the first LIGO detectors reach a couple of events per year and our most pessimistic estimate for advanced LIGO detectors exceed $\simeq 10$ events per year.

Subject headings: binaries: close — gravitational waves — stars: evolution, formation, neutron, black hole

1. INTRODUCTION

Gravitational waves are a natural consequence of Einstein's theory of general relativity (Einstein 1916, 1918). Indirect evidence for their existence came first from observations of the orbital decay of the Hulse-Taylor binary pulsar (Hulse & Taylor 1974, 1975a, 1975b; Taylor & Weisberg 1982, 1989). Direct detection though and analysis of gravitational-wave sources are expected to provide a unique insight to one of the least understood of the fundamental forces. They will also allow us to investigate the physical properties of astronomical objects that so far have been elusive because they do not emit any electromagnetic radiation (e.g., double black holes in isolation).

A number of interferometers designed for gravitational-wave detection are currently in operation, being developed, or planned. First results from the Japanese instrument TAMA300 have already been reported (Tagoshi et al. 2001). More advanced ground-based observatories are under development or in the commissioning phase, i.e., the US Laser Interferometer Gravitational-wave Observatory (LIGO; Abramovici et al. 1992), the British/German GEO-600 Observatory (Danzmann et al. 1995), the French/Italian VIRGO project (Caron et al. 1995), and the Australian ACIGA project (Sandeman 1998). Also future space missions are being planned, such as Laser Interferometer Space Antenna (LISA; Bender et al. 2000), a

joint project of ESA and NASA with the launch planned for 2009.

Astrophysical sources of gravitational radiation relevant to ground-based interferometers include: inspiraling double compact objects, binary stars, rotating neutron stars, neutron star instabilities, supernovae, supermassive black holes and stochastic background (for a review see Thorne 1987). Some of the most promising candidates are the inspiral and coalescence of double compact objects (DCO), such as NS-NS, BH-NS, and BH-BH binaries. Successful detection of these sources at reasonable event rates depends not only on the instrument sensitivity and the strength of the gravitational-wave signals, but also on the coalescence rates and the physical properties of the sources out to the maximum distances of reach of a given instrument.

Coalescence rates of double compact objects have been investigated by a number of different groups. For NS-NS binaries the rates can be calculated in two ways: (1) theoretically, based on the predictions of binary population synthesis calculations (e.g., Bethe & Brown 1998; Portegies Zwart & Yungelson 1998; Bloom, Sigurdsson & Pols 1999; Belczynski & Bulik 1999; Fryer, Woosley & Hartmann 1999) or (2) empirically, based on the observed sample of Galactic binary pulsars (e.g., Narayan, Piran, & Shemi 1991; Phinney 1991; Curran & Lorimer

1995; Arzoumanian, Cordes & Wasserman 1998; Kalogera et al. 2001; Kim, Kalogera, & Lorimer 2001). At present both methods appear burdened with significant uncertainties, the theoretical approach due to the many poorly constrained evolutionary model parameters, and the empirical estimates due to small-number sample of observed NS-NS systems (for a more detailed discussion see Kalogera et al. 2001). Predictions for BH-NS and BH-BH binaries can be obtained only from theoretical calculations, since no such systems have yet been observed. Accurate predictions for BH binaries are even harder to obtain, as the evolution of high-mass stars still challenge our understanding. Several results of population synthesis calculations have been presented in the literature, for BH-NS systems: Fryer et al. (1999); Belczynski, Bulik & Zbijewski (2000); Portegies Zwart & Yungelson (1998), and for BH-NS and BH-BH systems: Lipunov, Postnov & Prokhorov (1997); De Donder & Vanbeveren (1998); Nelemans, Yungelson & Portegies Zwart (2001b).

Given the history of population synthesis calculations, one may wonder what is the purpose on another set of models of the formation of double compact objects. The primary goal of this present study is to investigate the relevant formation processes in the light of recent developments in the evolution of compact object progenitors in binaries, and to clearly identify classes of formation channels, their origin, and their relative contributions. We focus not just on predicted rates, but at some level more importantly on the physical properties of formed binaries. Our parameter study is targeted to uncovering the systematic uncertainties as well as identifying those (qualitative) properties that appear to be robust. Investigation of these properties will help in characterizing the range of possible gravitational-wave signals and identification of their origin will allow reevaluating our results in the future as our understanding of model unknowns improves. As part of our analysis we also examine the implications of common-envelope phases involving helium stars and as a result we identify a number of new formation channels with important implications for the properties of double compact objects¹. Even though stellar structural characteristics may tentatively support such common-envelope phases late in the evolution of helium stars, we note that detailed hydrodynamical calculations will be needed to assess the viability of such phases involving helium stars or pairs of evolved stars as it has been assumed also in earlier studies (see Fryer et al. 1999; Nelemans et al. 2001a).

Our paper is organized as follows: In §2, we present a detailed description of our population synthesis code (named *StarTrack*). In §3 we: describe the extent of our parameter study (§3.1), discuss the statistical accuracy of our calculations (§3.2), present the formation paths of double compact objects (§3.3), and analyze in detail their properties (§3.4) and coalescence rates (§3.5) for a large number of different models. In §4, we discuss the impli-

cations of the most important of our results and conclude with prospects for gravitational-wave detection by ground-based interferometers.

2. POPULATION SYNTHESIS MODEL

2.1. *Single-Star Evolution*

2.1.1. *Overview*

In all the population synthesis models, we employ the analytic formulae derived by Hurley, Pols & Tout (2000, hereafter HPT) to model the evolution of single stars. These formulae represent fits to results from a large number of stellar evolution models calculated by Pols et al. (1998), using the Eggleton stellar evolution code (Eggleton 1971, 1972, 1973; latest updates and input physics described in Han, Podsiadlowski & Eggleton 1994 and Pols et al. 1995).

The HPT formulae² allow us to calculate the evolution of a star given its Zero Age Main Sequence (ZAMS) mass and its metallicity (Z). Stellar evolution is followed from ZAMS through a sequence of evolutionary phases depending on the initial (ZAMS) stellar mass: Main Sequence (MS), Hertzsprung Gap (HG), Red Giant Branch (RG), Core Helium Burning (CHeB), Asymptotic Giant Branch (AGB), which is further divided into Early AGB (EAGB) and Thermally Pulsing AGB (TPAGB), and for stars stripped off their hydrogen-rich layers: Helium Main Sequence (HMS), Helium Giant Branch (HGB). We end the evolutionary calculations at the formation of a stellar remnant: a white dwarf (WD), a neutron star (NS) or a black hole (BH). During the evolution we can track some of the basic stellar parameters: radius, luminosity, stellar mass, and core mass.

These single star models include the effects of mass loss due to stellar winds as described in HPT. Mass loss rates are adopted from the literature for different evolutionary phases. For H-rich stars on MS (Nieuwenhuijzen & de Jager (1990); using Z dependence of Kudritzki et al. 1989), for RGB (Kudritzki & Reimers 1978) and AGB (Vassiliadis & Wood 1993) stars, and for Luminous Blue Variables (HPT). For He-rich stars W-R, mass loss is included using rates derived by Hamann, Koesterke & Wessolowski (1995) and modified by HPT. Given the importance of single star winds in the formation of compact objects (e.g., Brown, Weingartner, & Wijers 1996; Ergma & van den Heuvel 1998; Fryer & Kalogera 2001), we examine this element of single star evolution and calculate synthesis models with varying strengths of stellar winds.

We have introduced two modifications to the HPT formulae concerning the treatment of (i) Helium-star evolution, and (ii) final remnant masses. These are described in detail in the next two subsections.

2.1.2. *Helium Star Evolution*

¹After the submission of this paper to *ApJ*, an early paper by Tutukov & Yungelson (1993) came to our attention. In this paper the authors allow for mass transfer from helium stars without a merger, although not through CE evolution. There is qualitative agreement between their and our results, however we point out that there are many differences in the binary evolution modeling (e.g., Tutukov & Yungelson do not account for any kicks to NS or BH not for hypercritical accretion, and many more). We also found out that CE evolution for low-mass helium stars has been discussed qualitatively in the past, in the context of the formation of NS-NS systems and X-ray binaries (van den Heuvel 1992; Taam 1996).

²We implemented the formulae into a *C* code, compared the results of our implementation with the original HPT *Fortran* subroutines for ZAMS masses 0.5–100 M_{\odot} and for metallicities: $Z = 0.0001 - 0.03$, and found perfect agreement.

After core helium exhaustion low-mass helium stars expand significantly and develop a “giant-like” structure with a clearly defined core and a convective envelope (Delgado, & Thomas 1981; Habets 1987; Avila-Reese 1993; Woosley, Langer, & Weaver 1995). Radial expansion is very important for stars in binaries as it may lead to mass transfer episodes. Low-mass evolved helium stars with convective envelopes possibly transfer mass on a dynamical time scale, and as a consequence a common envelope (CE) phase may ensue³. On the other hand, relatively massive helium stars do not develop deep convective envelopes and do not experience any significant radial expansion. Even if they happen to initiate mass transfer (MT), they respond differently to mass loss and a CE phase is not likely.

Based on the HPT formulae, the implied upper mass limit for helium stars to develop deep convective envelopes is $M_{\text{conv}} \sim 2.2 M_{\odot}$, which we consider to be rather low. We have examined in detail models of evolved helium stars (Woosley 1997, private communication) and found that helium stars below $4.0 M_{\odot}$ have deep convective envelopes, whereas slightly more massive helium stars ($\sim 4\text{--}4.5 M_{\odot}$) still form convective envelopes, although shallower. As an example, an evolved helium star of $M = 2.5 M_{\odot}$ develops a deep convective envelope reaching down almost to the core through 90% of the stellar radius. Based on this, for our standard model, we adopt $M_{\text{conv}} = 4.5 M_{\odot}$ for an evolved helium star to develop a deep convective envelope. However, in face of the uncertainties and the importance of helium-star evolution, we treat this value as a model parameter and include it in our parameter study. Throughout this paper we refer to the evolved helium stars with $M \leq M_{\text{conv}}$ as low-mass helium stars/giants (or low-mass HGB stars) and to the stars with $M > M_{\text{conv}}$ as massive helium stars/giants (or massive HGB stars). We note that, apart from the issue of convective envelopes, a comparison in terms of radial evolution alone between the HPT formulae and other published models of helium stars (e.g. Habets 1987) shows excellent agreement, so we adopt these formulae in calculating stellar radii. Detailed discussion of helium star evolution in context of double compact objects formation is given in Belczynski & Kalogera (2001).

2.1.3. Remnant Masses

The masses of NS and BH calculated by HPT are *very* small. For progenitors of $M_{\text{zams}} = 40\text{--}100 M_{\odot}$, they obtain final remnant masses in the range $\simeq 1.8\text{--}2.0 M_{\odot}$, (see their Figure 20). On the other hand, measurements of BH masses in binaries, although still highly uncertain, yield much higher values: $\sim 3\text{--}20 M_{\odot}$ (Orosz et al. 2001; McClintock et al. 2001; Froning & Robinson 2001; Wagner et al. 2001; Table 1 of Fryer & Kalogera 2001 and references therein). The HPT analytic formulae are based on the stellar models evolved at least to the formation of a carbon-oxygen (CO) core, and these core masses are in good agreement with earlier stellar models (e.g., Schaller et al. 1992). Therefore, instead of using their somewhat arbitrary prescription (see their equation [75]) for NS and

BH masses, we adopt a different formula derived on the basis of core-collapse hydrodynamical calculations (Fryer 1999, Fryer & Kalogera 2001). We note that there are still many uncertainties associated with the physics of the supernova mechanism, and there is still disagreement among research groups about the cause of the explosion (e.g., Liebendoerfer et al. 2001 and references therein). For our study we choose the specific core-collapse models, primarily because they are the only one available in the literature that allow us to calculate the remnant mass taking into account fallback, in a self-consistent way.

We adopt the HPT formulae to calculate the final CO core mass of a star, and we use stellar models of Woosley (1986) to obtain a final FeNi core mass as a function of the CO core mass. At the time of core collapse, we describe the star with its current mass M , the final CO core mass M_{CO} and the final FeNi core mass M_{FeNi} . To estimate the mass of the remnant formed, we follow the results of hydrodynamical calculations of core collapse (Fryer 1999). These calculations have shown that (i) progenitors with $M_{\text{zams}} \leq 20 M_{\odot}$ do not experience any significant fall back and apart from the collapsing core, the stellar outer layers are expelled as SN ejecta, (ii) for progenitors with $M_{\text{zams}} \geq 42 M_{\odot}$, the whole pre-collapse star directly implodes to form a BH and no SN event takes place, (iii) for intermediate progenitor masses remnants are formed through an initial core collapse and subsequent partial fall back. The outcome of a given core-collapse event is found to depend primarily on the core mass of the collapsing star and not on the initial (ZAMS) stellar mass. Taking into account that the stellar population models used by Fryer (1999) were of constant mass (without wind or mass transfer effects; see Fryer & Kalogera 2001), we have developed a prescription based on CO core masses. Using the HPT formulae we obtain $M_{\text{CO}} = 5 M_{\odot}$ for $M_{\text{zams}} = 20 M_{\odot}$, and $M_{\text{CO}} = 7.6 M_{\odot}$ for $M_{\text{zams}} \leq 42 M_{\odot}$, for $Z = 0.02$ using the standard wind mass loss prescription. We then calculate the mass of the remnant as follows:

$$M_{\text{rem}} = \begin{cases} M_{\text{FeNi}} & M_{\text{CO}} \leq 5 M_{\odot} \\ M_{\text{FeNi}} + f_{\text{fb}}(M - M_{\text{FeNi}}) & 5 < M_{\text{CO}} < 7.6 \\ M & M_{\text{CO}} \geq 7.6 M_{\odot} \end{cases} \quad (1)$$

where f_{fb} is the *fall-back* factor, i.e. the fraction (from 0 to 1) of the stellar envelope that falls back. In Figure 1, we present the initial-remnant mass relation, for single Population I stars ($Z = 0.02$), and for three different wind mass-loss rates.

The top panel of Figure 1 shows the initial-remnant mass relation for our standard prescription of wind mass-loss rates.

Stars of $M_{\text{zams}} = 0.5\text{--}0.8 M_{\odot}$ form helium white dwarfs (He WD), of $M_{\text{zams}} = 0.8\text{--}6.3 M_{\odot}$ form carbon-oxygen white dwarfs (CO WD), and of $M_{\text{zams}} = 6.3\text{--}8.0 M_{\odot}$ form oxygen-neon white dwarfs (ONe WD).

For stars with initial mass M_{zams} in excess of $8 M_{\odot}$, the stellar core mass exceeds the Chandrasekhar mass and

³We note that whether a common-envelope phase develops as well as the outcome depends not only on the presence of convective envelopes but also on the detailed stellar structure (density profile, masses of the envelope relative to the core) as well as the mass ratio in the binary and the spin evolution of the envelope during the mass-transfer episode (Fryer 2001; Rasio 2001; Taam 2001, private communications). The hydrodynamics of mass transfer from helium stars with appropriate masses and companions have never been studied so far, but such studies will be necessary to determine the outcome of these evolutionary phases. In the present study we account for such a possibility and examine its implication for the DCO populations.

once nuclear reactions stop the core collapses into a NS. For $M_{\text{zams}} = 8 - 20.0 M_{\odot}$, the outer stellar layers (on average $\sim 7 M_{\odot}$) are lost in SN explosion, and no fall back takes place. This part of the initial-remnant mass relation is characterized by a slow increase of the NS mass with increasing M_{zams} , as more massive progenitors form only slightly more massive cores, which eventually collapse to NS.

Partial fall back is initiated above $M_{\text{zams}} = 20.0 M_{\odot}$ and the amount of material accreted back onto the collapsing core increases linearly with increasing progenitor mass. Due to the fall back the initial-remnant mass relation significantly steepens over $M_{\text{zams}} = 20.0 M_{\odot}$. Note that the remnant mass reaches maximum NS mass $M_{\text{max}}^{\text{NS}} = 3.0 M_{\odot}$ at $M_{\text{zams}} = 20.7 M_{\odot}$, so in this model the most massive NS are formed through fall back.

For $M_{\text{zams}} \sim 25 M_{\odot}$ there is a small drop and a subsequent flattening of the initial-remnant mass relation. At this and higher progenitor masses stellar winds strip star completely of its hydrogen layers. Once a naked helium star is formed the wind mass loss rate increases significantly. The effect of wind mass loss enhancement with increasing M_{zams} diminishes both the final core mass and the pre-collapse envelope mass (the fall back mass reservoir) and therefore decreases the remnant mass. With increasing M_{zams} the fall back factor f_{fb} goes up, but because of the helium star mass loss rate effect on the pre-collapse star, the remnant mass does not increase as fast as before.

Stars more massive than $M_{\text{zams}} = 42 M_{\odot}$ collapse directly into a BH at the end of their evolution. The initial-remnant mass relation flattens out even more. This is a consequence of a “fall-back saturation”. The fall back is now complete ($f_{\text{fb}} = 1$) and cannot increase any more with progenitor mass, as it was the case for less massive stars in the range of partial fall back. Now the remnant mass depends only on the pre-collapse mass, which increases rather slowly with progenitor mass as the wind mass loss rate increases also with M_{zams} .

Stars over $M_{\text{zams}} \sim 48 M_{\odot}$ reach high luminosities and radii exceeding the Humphreys-Davidson limit (Humphreys & Davidson 1994) and enter the Luminous Blue Variable (LBV) phase. During the LBV phase stars lose mass at a very high rate, which result in a sudden drop in the initial-remnant mass relation. Due to this significant mass loss, stars over $M_{\text{zams}} = 49 M_{\odot}$ form smaller cores and experience partial fall back at core collapse. The effect of LBV-like mass loss takes over the effect of an overall increase of CO core mass (and thus remnant mass) with M_{zams} , and it influences the remnant mass in two ways. First, LBV-like mass-loss rates increase with increasing stellar mass leading to a decrease of remnant masses. Second, for higher stellar ZAMS masses, the LBV phase begins earlier in the life of a star. Hence, the stars are stripped of their hydrogen layers earlier, and less massive helium stars are formed, leading to a decrease in remnant masses. In the standard wind model, remnant masses reach their local minimum at $M_{\text{zams}} = 52.5 M_{\odot}$, when the LBV phase sets in the earliest possible, i.e., at the beginning of Hertzsprung gap. For more massive stars, the overall increase of remnant mass with progenitor mass dominates once again, as CO core masses steadily grow and the contribution of fall back steadily increases.

For progenitors with $M_{\text{zams}} \geq 72.3 M_{\odot}$ remnants are once again formed through complete fall back and the initial-remnant mass relation flattens out, following the slow increase of pre-collapse mass with M_{zams} .

In the middle panel of Figure 1, results are shown for Wolf-Rayet mass-loss rates reduced by a factor of two. The initial-remnant mass relation changes only slightly from that of the top panel as partial fall back at high ZAMS masses is eliminated. As expected, compact objects are slightly more massive and the maximum BH mass increases from $\sim 11 M_{\odot}$ (top panel) to $\sim 15 M_{\odot}$ (see also Wellstein & Langer 1999).

In the bottom panel of Figure 1, results are shown for the case of all wind mass-loss rates reduced by a factor of two, and we find some significant changes in the initial-remnant mass relation. First, as expected, the compact object masses are higher than for both models described above; the maximum mass of the compact object in this model increases to $\sim 19 M_{\odot}$. Second, the qualitative shape of the relation changes. As in the standard wind model, we find two sudden drops in the relation, with the first one being more prominent than before. In the standard model the first drop corresponds to the stripping star of its hydrogen layers and the formation of a helium star, whereas the second drop is related to the onset of LBV phase for very luminous and extended stars. These two effects lead to significantly increased mass loss rates, and thus decrease the remnant masses. Detailed examination of this model reveals that in the bottom panel, the first drop corresponds to the onset of the LBV phase and the second to the helium star formation. Since all wind rates are reduced and wind mass loss rates depend strongly on the stellar mass, helium stars are exposed only for stars of higher initial mass. Consequently, stars with much lower initial masses (below $M_{\text{zams}} \sim 40 M_{\odot}$) retain their hydrogen-rich layers and are able to evolve to higher luminosities and larger radii, which shifts the onset of the LBV phase to lower initial masses. Another difference is that, the immediate progenitors of compact objects tend to be more massive, and therefore direct BH formation spans much wider range of initial masses than for the standard wind model. These more massive progenitors form more massive CO cores, and none of the factors that decrease pre-collapse masses are strong enough to decrease the CO core masses below $7.6 M_{\odot}$ (see eq. 1). Consequently, BH formation through partial fall back does not occur for two separate M_{zams} ranges (as is the case for $M_{\text{zams}} = 21-42$ and $48-72 M_{\odot}$ in the standard wind model).

2.2. Binary Evolution

2.2.1. Overview

We use Monte Carlo techniques to model the evolutionary history of double compact objects and study their physical properties. We generate a large number ($N \geq 10^6$) of primordial binaries, drawing their initial physical parameters (component masses, orbital separations and eccentricities) from assumed distributions described in §2.2.2. Besides that, Monte Carlo events are used to *i*) set the time of birth of each binary in the disk of our Galaxy (for constant star formation rate the probability distribution of the birth time is flat in the range $0 - 10$ Gyr), *ii*) set the kick velocity direction and magnitude each NS or

BH receives when formed in an asymmetric SN explosion and *iii*) set the position along the binary orbit in which SN take place. In all other instances, the evolution is modeled based on a set of formulae and prescriptions (described in what follows) that depend on the binary properties.

The evolution of each system is followed in a number of time steps. The time step is chosen to be a small fraction (≤ 0.01) of the evolutionary phase lifetime of the more rapidly evolving stellar component, making sure that the relative change in radius is always less than 10%. We start the evolution of a given binary with two components at ZAMS, and we stop the calculation when the two components have formed stellar remnants or when a merger occurs or when the system has reached the present time, i.e., the sum of its age and its birth time is equal to 10 Gyr). The evolution of each binary component in isolation is calculated as described in § 2.1, and a number of evolution effects on the binary orbit (e.g., mass and angular momentum losses due to stellar winds) are taken into account. At every evolutionary time step, we check for possible binary interactions. If any of the components fills its Roche lobe, we calculate the effects of mass transfer and possible mass and angular-momentum loss on the orbit. Depending on the masses of the components and their evolutionary stage, we apply appropriate prescriptions for the modeling of different mass transfer events (as described in § 2.2.4). If the binary survives the mass-transfer event (i.e., both stellar components fit within their Roche lobes), we continue to model its evolution. At every time step, we also check the single-star models (see § 2.1) to determine if any of the components has finished its nuclear evolution, and has turned into a compact remnant. If a remnant is born in a SN explosion, we calculate the effects of SN kicks and mass loss on the binary orbit (both circular and eccentric). If a binary is disrupted in SN explosion, we follow the single-star evolution of components, otherwise we continue with the evolution of the whole binary. Once a binary consists of two remnants, we calculate its merger lifetime, i.e., the time until the components merge due to gravitational radiation and associated orbital decay, and we study the properties and formation rates of different classes of binaries containing compact objects. In what follows we describe in detail prescriptions for binary evolution and all model assumptions as chosen for our standard model. The assumptions for models in our parameter study are given in § 3.1.

2.2.2. Distributions of Initial Parameters

A binary system is described initially by four parameters: the mass of the primary M_1 (the initially more massive component), the mass ratio $q = \frac{M_2}{M_1}$, where M_2 is the mass of the secondary (initially less massive component), the semi-major axis A of the orbit, and the orbital eccentricity e . We assume that the initial distributions of these parameters are independent.

For both, single stars and binary system primaries, we adopt the initial mass function derived by Scalo (1986),

$$\Psi(M) \propto M^{-2.7}, \quad (2)$$

in the mass range $M_1 = 5 - 100 M_\odot$ relevant to compact object formation. Although, for single stars, the minimum initial mass for NS formation is $\simeq 8 M_\odot$ (or maybe

higher), a lower limit of $5 M_\odot$ ensures that we do not miss any NS progenitors due to binary evolution. Mass transfer in a binary can increase any component's mass, and effectively decrease the minimum initial mass of NS progenitors. Let us consider a border-line case of the lowest-mass primary ($5 M_\odot$) and the corresponding highest-mass secondary ($5 M_\odot$). The primary evolves off the MS with a helium core of $\sim 1 M_\odot$ and $\sim 4 M_\odot$ in its envelope. For our standard model of binary evolution, we assume that only half of the donor envelope can be accreted by its companion (see § 2.2.4). So for this border-line case, the initial secondary mass can be increased to $\leq 8 M_\odot$, or for all other cases, to masses smaller than the mass limit for NS formation.

Following Kuiper (1935), we assume a flat mass ratio distribution,

$$\Phi(q) = 1 \quad (3)$$

in the range $q = 0 - 1$. Given value of the primary mass and the mass ratio, we obtain the mass of the secondary $M_2 = qM_1$. We evolve only systems with secondaries of $M_{\text{zams}} \geq 0.5 M_\odot$, as less massive stars will not evolve within a Hubble time.

The distribution of the initial binary separations is assumed to be flat in the logarithm (Abt 1983),

$$\Gamma(A) \propto \frac{1}{A}, \quad (4)$$

where A ranges from a minimum value, such that the primary fills its Roche lobe, up to $10^5 R_\odot$.

We adopt the thermal-equilibrium eccentricity distribution for initial binaries,

$$\Xi(e) = 2e, \quad (5)$$

in the range $e = 0 - 1$ (e.g., Heggie 1975; Duquennoy & Mayor 1991).

2.2.3. Evolution of Binary Orbit

Tidal circularization of binary orbits takes place in systems in where the size of any component is comparable to the binary separation (Zahn 1978). This condition is satisfied when at least one of the binary components evolves beyond the MS or the initial binary separation is small. To calculate the effects of tidal circularization on a binary orbit we follow the prescription developed by Portegies Zwart & Verbunt (1996): circularization occurs, if the stellar radius of one component is larger than 0.2 of the periastron binary separation. The orbital elements (A, e) change under conservation of angular momentum until the new periastron distance is equal to 5 stellar radii of the component driving the circularization, or until the orbit is circularized ($e = 0$). We also assume that tidal circularization takes place instantaneously (i.e. in one evolutionary time step).

Stellar winds affect binary orbits through mass and angular-momentum losses. Assuming a spherically symmetric stellar wind, which carries away the specific angular momentum of the mass-losing star, and a circular orbit

(Jeans-mode mass loss), the change in the binary separation is given by

$$A(M_1 + M_2) = \text{const.} \quad (6)$$

For eccentric orbits the change in A is rather similar (Vanbeveren, Van Rensbergen & De Loore 1998).

Orbits are also affected by mass transfer events and SN explosions. The treatment of these effects is described in the subsections that follow.

2.2.4. Mass Transfer Events

When one of the binary components fills its Roche lobe, mass is transferred to its companion through the inner Lagrangian point. The responses of both components and the orbit as well as the outcomes of MT phases depend on the masses and evolutionary stages of the two stars. In our calculations we distinguish between (i) dynamically stable, in general non-conservative (allows for mass and angular-momentum loss from the system) mass transfer, and (ii) dynamically unstable mass transfer that leads to common envelope evolution (for more details and reviews see, e.g., Ostriker 1975, Paczynski 1976, Iben & Livio 1993, Rasio & Livio 1996; Taam & Sandquist 2000). We are interested in the end products of MT events, and therefore, we assume that MT takes place instantaneously. Following any MT event, we update the binary component masses and evolutionary stages and calculate their radii⁴. Using the post-MT radii and separation, we examine whether systems survived the MT event and a component merger was avoided.

Non-conservative Stable Mass Transfer. This phase is implemented if (i) the donor is a MS or HMS star transferring mass to an accretor of any evolutionary stage, or (ii) the donor is a H-rich or He-rich giant and the accretor is not, and the following is true

$$M_{\text{don}} \leq c_r M_{\text{acc}} \quad (7)$$

where $M_{\text{don}}, M_{\text{acc}}$ are the donor and accretor masses at the beginning of the MT episode. Based on earlier results obtained by Hjellming & Webbink (1987), Kalogera & Webbink (1996) and Ritter (1999), $c_r = 2.5$ if the donor is in HG and the accretor is a MS star, and $c_r = 1$ in all other cases.

During this type of MT episodes, part of the mass lost by donor (f_a) is accreted onto the companion, and the rest is lost from the system with a specific angular momentum equal to $2\pi j A^2/P$ (Podsiadlowski, Joss & Hsu 1992). The corresponding orbital separation A change can be calculated for $f_a = 0$ from:

$$\frac{A_f}{A_i} = \frac{M_{\text{don}}^f + M_{\text{acc}}^f}{M_{\text{don}}^i + M_{\text{acc}}^i} \left(\frac{M_{\text{don}}^f}{M_{\text{don}}^i} \right)^{2(j-1)} \exp \left[\frac{2j(M_{\text{don}}^f - M_{\text{don}}^i)}{M_{\text{acc}}^i} \right], \quad (8)$$

⁴For bare CO cores, in the absence of any published models, we adopt a fixed radius of $0.01 R_{\odot}$. We find that variation of this assumed value does not affect our results in any appreciable way (even for an increase of this radius by an order of magnitude).

⁵The issue of progenitors of Type Ia SN is still not resolved (e.g., Branch et al. 1995). However, our assumption of the occurrence of Type Ia SN does not influence our results. Since accreting WD companions are less massive or of comparable mass, even if WD were to collapse to NS due to accretion, the chance of forming double compact objects is vanishing

and for $f_a > 0$ from:

$$\frac{A_f}{A_i} = \frac{M_{\text{don}}^f + M_{\text{acc}}^f}{M_{\text{don}}^i + M_{\text{acc}}^i} \left(\frac{M_{\text{don}}^f}{M_{\text{don}}^i} \right)^{c_1} \left(\frac{M_{\text{acc}}^f}{M_{\text{acc}}^i} \right)^{c_2}, \quad (9)$$

where

$$c_1 \equiv 2j(1 - f_a) - 2,$$

$$c_2 \equiv -\frac{2j}{f_a}(1 - f_a) - 2,$$

$$M_{\text{acc}}^f = M_{\text{acc}}^i + f_a(M_{\text{don}}^i - M_{\text{don}}^f),$$

and where $M_{\text{acc}}, M_{\text{don}}$ indicate binary component – donor and accretor masses, and the indices i, f denote the initial and final values, respectively. For our standard model, we assume that half of the mass lost from the donor is also lost from the system ($1 - f_a = 0.5$) with specific angular momentum $j = 1$.

For MS and HMS donors, we follow the MT episode in small ($< 1\%$) mass increments and we update the stellar masses and radii as well as the orbital separation and the Roche-lobe radii. Mass transfer is terminated when, for both stars, the Roche-lobe radii exceed the stellar radii. We also take into account possible rejuvenation of the accretor (as described in HPT) and update its radius and core mass. If during this mass transfer phase the donor mass decreases below $0.5 M_{\odot}$ for MS stars or below $0.3 M_{\odot}$ for HMS star, we terminate our calculations for the specific system, since such low-mass stars will not end their evolution in a Hubble time. For donors beyond the MS, we assume that the entire stellar envelope is lost and the final donor mass is equal to its core mass: He core or CO core mass for H-rich or He-rich stars, respectively.

The mass-ratio criterion for stable mass transfer (see eq. 7) also accounts for cases where the accretor is a NS or BH (see Kalogera & Webbink 1996; Kalogera 2000). We extend this treatment also to WD and allow for non-conservative mass transfer in cases where the criterion is satisfied. When WD masses exceed $1.44 M_{\odot}$ (Chandrasekhar mass according to our stellar models) we assume that a Type Ia SN occurs⁵. We also allow for accretion-induced collapse of NS to BH and we treat the boundary $M_{\text{max}}^{\text{NS}}$ as a model parameter. It is clear that our treatment of dynamically stable accretion onto compact objects does not include some important aspects (e.g., Eddington-limited accretion, transient systems), but it turns out that these MT phases are not crucial to double compact object formation.

Conservative Mass Transfer. In general, we assume that dynamically stable mass transfer is non-conservative and we include the case of conservative mass transfer (no mass or angular-momentum loss from the system) in our parameter study. In this case, $f_a = 1$ and equation 9 reduces to (e.g. Verbunt & Van den Heuvel 1995),

$$\frac{A_f}{A_i} = \left(\frac{M_{\text{don}}^i M_{\text{acc}}^i}{M_{\text{don}}^f M_{\text{acc}}^f} \right)^2. \quad (10)$$

Standard Common Envelope Phase. In all cases where criterion 2.7 is not satisfied, the donor has reached the giant branch, and the accretor is either a MS, HMS, WD or a high mass He-rich giant branch star, we expect mass transfer to be dynamically unstable and a common envelope spiral in and ejection to occur (Iben & Livio 1993). We assume that, during the CE phase, the donor loses its entire envelope and the spiraling-in companion does not accrete any of the envelope material.

We base our treatment on the energy formalism of the CE evolution (Webbink 1984), where the envelope is ejected on the expense of the binary orbital energy, and a tight post-CE system forms. The final orbital separation A_f is calculated using,

$$\alpha_{ce} \left(\frac{GM_{don}^f M_{acc}}{2A_f} - \frac{GM_{don}^i M_{acc}}{2A_i} \right) = \frac{GM_{don}^i M_{don,env}}{\lambda R_{don,rl}} \quad (11)$$

where, M_{don} and M_{acc} are masses of the donor and its companion, $M_{don,env}$ is mass of donor's envelope, $R_{don,rl}$ is the Roche lobe radius of the donor, and the indices i, f denote the initial and final values, respectively. Parameter λ describes the central concentration of the giant (de Kool 1990; Dewi & Tauris 2000). The right hand side of equation 11 expresses the binding energy of the donor's envelope, the left hand side represents the difference between the final and initial orbital energy, and α_{ce} is the CE efficiency with which orbital energy is used to unbind the stellar envelope. If the calculated final binary orbit is too small to accommodate the two stars then a merger occurs. In our calculations, we combine α_{ce} and λ into one CE parameter, and for our standard model, we assume that $\alpha_{ce} \times \lambda = 1.0$.

Double Common Envelope Phase. Brown (1995) suggested that if two binary components are giants with convective envelopes and mass transfer is initiated, then a double CE can form, where the two stellar cores spiral in the combined stellar envelopes. As in the case of low-mass helium stars, hydrodynamical studies of such a phase have not been undertaken, and we note that, despite its plausibility, the validity of such an assumption has not been demonstrated in detail (see also footnote in § 2.1.2). We use an analogue of equation 11 to describe the energy balance of a double CE and to calculate the change of binary separation A ,

$$\alpha_{ce} \left(\frac{GM_1^f M_2^f}{2A_f} - \frac{GM_1^i M_2^i}{2A_i} \right) = \frac{GM_1^i M_{1,env}}{\lambda R_{1,rl}} + \frac{GM_2^i M_{2,env}}{\lambda R_{2,rl}} \quad (12)$$

where M_1, M_2 are the two donor masses, $M_{1,env}, M_{2,env}$ are their envelope masses and other symbols have the same meaning as in equation 11 (see also Nelemans et al. 2001a).

Common Envelope with Hyper-critical Accretion. It has been suggested that if a NS or BH evolves through a CE phase, the compact object may accrete significant amounts of material because of hyper-critical accretion (Blondin 1986; Chevalier 1989, 1993; Brown 1995). Bethe & Brown (1998) derived an analytic scheme for the evolution of the binary orbit and the increasing mass of the accreting compact object, under the assumption that the mass of the

compact object is much smaller than the mass of the giant. However, for a large fraction of CE events this assumption is not justified, e.g., binaries with NS and a low-mass He-rich giant, or with a $\sim 5 - 10 M_\odot$ BH and a relatively massive giant companion.

In *StarTrack*, we relax the simplifying assumption made by Bethe & Brown (1998) and derive a formulation that can be applied to CE phases with hyper-critical accretion for any compact object and companion masses. This new formulation involves the numerical solution of a set of ordinary differential equations for the final compact object mass and orbital separation of the post-CE system. This non-approximate solution, results in tighter post-CE systems and lower mass compact objects compared to the analytic expression of Bethe & Brown (1998). We present the detailed derivation in Appendix A.

Unmodeled cases. There are two cases of binary interactions that are not covered by the above MT prescriptions, as we cannot readily foretell the outcome of some mass transfer events. We do not follow the subsequent evolution of binaries going through such events, but we keep a record of their occurrences. For both types of unmodeled MT events, the fraction of primordial binaries that encounter such events is below 0.1% for all our models.

These two types of unmodeled events are: (i) Unevolved donor with an evolved companion (i.e., giant with convective envelope). This configuration is encountered very rarely, as usually it is the giants that fill their Roche lobes. (ii) Compact objects accreting from massive evolved helium stars (with radiative envelopes). We expect that most of these cases lead to stellar mergers. Moreover, if any two of MS, HMS or massive HGB stars fill their Roche lobes at the same time, the formation of a contact system is recorded, and the calculations for these systems are terminated⁶.

2.2.5. Core Collapse and Supernova Explosion Events

For each massive star, the time of core collapse is set by the single star models (taking though into account mass variations due to winds and binary interactions). When either component of a binary reaches this stage, we generate a random location in the orbit for the event to take place (note that for eccentric binaries this choice will affect the outcome, since the components' separation and relative velocities are different at different locations in the orbit). The core-collapse event is assumed to be instantaneous and the mass of the remnant is calculated using equation 1. Note that if the remnant is formed through complete fall back (leading always to direct BH formation), we do not expect a SN explosion (hence no kick and no mass loss) and the orbit remains unchanged (Fryer 1999). When BH is formed through partial fallback we treat the event as a SN explosion (see Podsiadlowski et al. 2001).

We calculate the effect of a SN event on binaries in three steps: (i) We estimate the mass of the remnant. The rest of exploding star is immediately lost from the binary (with the angular momentum specific to the exploding component). We assume that the ejecta do not have any effect on the companion (e.g., Kalogera 1996). (ii) We calculate

⁶We find that the fraction of contact systems formed is rather independent of the adopted evolutionary model and is in the range 4–6% of the total simulated binary population.

the compact object velocity which is the vector sum of the orbital velocity of the pre-collapse star at the orbital position and the kick velocity. The kick velocity is assumed to be randomly oriented and its magnitude is drawn from an assumed distribution. The kick magnitude is also scaled with the amount of material ejected in the SN explosion,

$$V_{\text{kick}} = (1 - f_{\text{fb}}) * V, \quad (13)$$

where V is the kick magnitude drawn from a given assumed distribution, and f_{fb} is a fall back parameter defined in §2.1.3, and the V_{kick} is the kick magnitude we use in our calculations. For NS remnants and no fall back ($f_{\text{fb}} = 0$) and $V_{\text{kick}} = V$. In our standard model we use a kick magnitude distribution very similar to the one derived by Cordes & Chernoff (1998): a weighted sum of two Maxwellians, one with $\sigma = 175 \text{ km s}^{-1}$ (80%) and the second with $\sigma = 700 \text{ km s}^{-1}$ (20%). This distribution accounts for the fact, that besides average velocity pulsars a significant fraction of neutron stars have velocities above 500 km s^{-1} (Arzoumanian, Cordes, & Chernoff 1997). (iii) We calculate the total energy (potential and kinetic) of the new orbit for the remnant (new velocity and mass, same relative position) and its companion. If the total energy is positive, then the system is disrupted, and its components will evolve separately. We calculate their subsequent evolution as single stars, but we do not follow their trajectories in the present study. If the total binary energy is negative, the system after SN explosion is bound, and we calculate its new parameters (e and A). We also check whether the two components have merged due to the SN mass loss and kick in which case we terminate the evolution. Finally, we calculate the post-SN center of mass velocity of a binary.

2.2.6. Orbital Decay Due to Gravitational Radiation

Once both components of a binary have ended their nuclear evolution and formed stellar remnants, their orbits change only due to angular momentum loss through gravitational radiation. We calculate the merger times of these binaries using the formalism developed by Peters (1964), the result of which is briefly described below.

The decay rates of eccentricity e and orbital separation A are combined to derive the eccentricity evolution with time $e(t)$ and integrate to the limit $e \rightarrow 0$ (as the system approaches merging, i.e., $A \rightarrow 0$):

$$t_{\text{merg}} = \frac{12}{19} \frac{c_0^4}{\beta} \times \int_0^{e_0} \frac{e^{29/19} [1 + (121/304)e^2]^{1181/2299} de}{(1 - e^2)^{3/2}}, \quad (14)$$

where e_0 and A_0 are the initial eccentricity and orbital separation,

$$c_0 = A_0 \frac{1 - e_0^2}{e_0^{12/19} [1 + (121/304)e_0^2]^{870/2299}},$$

$$\beta = \frac{64}{5} \frac{G^3 M_1 M_2 (M_1 + M_2)}{c^5},$$

and where G is the gravitation constant and c is the speed of light. In practice the limit $A \rightarrow 0$ (accompanied by

$e \rightarrow 0$) is unrealistic, since a merger occurs earlier, but the very final parts of this integration do not contribute significantly to the merger time, as the very late stages of inspiral proceed on very short timescales. For example, the merger time we calculate for PSR B1913+16 is within 1% of the result obtained by solving the system of two ordinary equations for the eccentricity and orbital separation (e.g., Junker & Schaefer 1992).

We note that, for a circular orbit, we obtain a merger time:

$$t_{\text{merg}} = a_0^4 / (4\beta). \quad (15)$$

2.2.7. Star Formation History and Binary Fraction

For most of our models, we assume that star formation has been continuous in the disk of our Galaxy for the last 10 Gyr as inferred from observations (e.g., Gilmore 2001) and as predicted by recent theoretical modeling (e.g., Kauffmann, Charlot & Balogh 2001). We start the evolution of a single or a binary system t_{birth} ago, and follow it to the present. The birth time t_{birth} is drawn randomly within the range 0–10 Gyr. In our parameter study, we examine a model of instantaneous star formation.

For most of our models, we also assume a binary fraction of $f_{\text{bi}} = 0.5$, which means that for any 150 stars we evolve, we have 50 binary systems and 50 single stars. We treat f_{bi} as a model parameter and include it in our parameter study. Finally, in all our models we assume solar metallicity $Z = 0.02$.

3. RESULTS

3.1. Population Synthesis Parameter Study

We perform an extensive parameter study in order to assess the robustness of our population synthesis results. In Table 1 we summarize all our models based on those assumptions that are different from our standard model (model A). Parameter values and adopted distributions in the standard model are as given in the two previous sections: §2.1 and §2.2.

In models marked with letter B, we use different distributions of SN kick magnitudes imparted to NS at birth. In model B1 we assume symmetric SN explosions, whereas in models B2–12 we draw kick velocities V_k from a single Maxwellian:

$$g(V_k) \propto V_k^2 \exp[-(V_k/\sigma)^2], \quad (16)$$

varying σ values in the range $10 - 600 \text{ km s}^{-1}$. In model B13 we use a kick distribution of the form suggested by Paczynski (1990):

$$f(V_k) \propto [1 + (V_k/\sigma)^2]^{-1}, \quad (17)$$

which allows for a significant fraction of low-magnitude kicks. We use $\sigma = 600 \text{ km s}^{-1}$, which gives a reasonable fit to the population of single pulsars in the solar vicinity (Hartman 1997).

In model C, compact objects (NS or BH) are not allowed to accrete any material in CE events. In models D1–2, we reduce our conservative maximum limit on the NS mass of $3 M_{\odot}$ down to 2 and $1.5 M_{\odot}$. Models E1–3 present evolution with different effective CE efficiencies ($\alpha_{\text{ce}} \times \lambda$). In

model F1, we significantly decrease the amount of material accreted by companions in non-conservative MT events, whereas in model F2, we examine the case of conservative mass transfer. In models G1–2, we vary the wind mass loss rates. In model G1, we decrease the wind mass loss rate by a factor of 2, for all stars and at all evolutionary stages, whereas in model G2, we enhance it by factor 2. In other words, we calculate the wind mass loss rate as described in § 2.1.1, and multiply it by f_{wind} given in Table 1. Model H1 corresponds to evolution with $M_{\text{conv}} = 4.0M_{\odot}$, the upper mass limit for helium giants with convective envelopes that would initiate a CE phase. Model H2 does not allow for CE evolution for any Roche-lobe filling helium stars regardless of their mass (effectively $M_{\text{conv}} = 0$). In model I, the star formation rate (SFR) is altered, and instead of continuous we assume a burst-like star formation history, with all stars being formed 10 Gyr ago. In model J, we use an initial mass function (IMF) with a Salpeter (1955) exponent of -2.35 , and in models K1–2, we vary the binary fraction of binary systems in the primordial stellar populations. In models L1 and L2, we vary the specific angular momentum of material lost during dynamically-stable MT events. In models M1 and M2, we use different distributions of initial binary mass ratios. Model N corresponds to the artificial case of evolution without allowing for the expansion of evolved helium stars. This model is nonphysical since low mass helium stars are known to evolve to giant-like stages and to significantly increase their radii (for a detailed discussion see Belczynski & Kalogera 2001 and references therein). We include this model in our parameter study only for the purposes of comparing our results to earlier studies that did not account for helium star radial evolution. In model O, we increase the mass range of compact object formation through partial fall back, resulting to no BH forming through a direct collapse.

3.2. Statistical Accuracy

Apart from the systematic uncertainties of our results which we examine with the broad parameter study discussed above, we also examine the statistical accuracy of our population synthesis models, to make sure that we do not burden the quantitative predictions with unnecessary uncertainties. To determine the intrinsic statistical accuracy of our synthesis models, we performed 30 different realizations of our standard model (A), each with $N = 10^6$ independently generated primordial binaries. We decide to limit ourselves to $N = 10^6$ runs, given our computational resources.

In Table 2, we present the results we obtained by comparing the 30 different runs. For each of the three DCO populations, we list the mean number of systems formed from the set of $N = 10^6$ runs, its standard deviation (as a percentage), as well as the maximum variation in the predicted numbers of systems. We find that the standard deviations do not exceed 10% for any type of DCO, whereas the maximum variation remains below 10% for the most frequent NS-NS binaries and below 30% for the least frequent population of BH-NS binaries. In what follows, we present results for our standard model using the combined total of these 30 runs (or their subgroups) and therefore statistical inaccuracies are greatly reduced and become insignificant compared to the systematic uncertainties. For

some of the other models in our parameter study (e.g., E1, G2) we also considered results from runs with more than 10^6 primordial binaries to ensure that our statistical errors remain well below 10% for all three DCO types.

3.3. Formation Paths of Double Compact Objects

We consider double compact objects with NS or BH (NS-NS, BH-NS or BH-BH binaries) with merger times shorter than 10^{10} yr, thus *coalescing* DCO. In our standard evolutionary model, the population of coalescing DCO is dominated by NS-NS systems (61%), with a significant contribution by BH-BH binaries (30%), and a small contribution by BH-NS objects (9%). In what follows we discuss the main qualitative characteristics of the important formation paths (with relative formation frequencies higher than 1%) as well as their origin.

In Table 3, we present the most important formation channels of coalescing DCO, for our standard model. Formation channels of NS-NS, BH-NS and BH-BH binaries are marked by NSNS, BHNS and BHBH, respectively, they are listed in order of decreasing relative formation frequency (second column) with respect to the whole DCO coalescing population. The details of each evolutionary sequence, i.e., MT episodes and SN explosions are also given. Results were obtained based on the evolution of 3×10^7 primordial binaries.

3.3.1. Populations of Double Neutron Stars

Using the *StarTrack* population synthesis code, we identified a number of new NS-NS formation channels (see below). This is a result of two improvements in the implementation of our population synthesis code, since our previous short study of the NS-NS formation (Belczynski & Kalogera 2001, hereafter BK01). First, we have replaced the approximate prescription suggested by Bethe & Brown (1998) for the hyper-critical accretion during CE phases, with a newly derived numerical solution (see Appendix). Second, we allow for hyper-critical CE evolution of low-mass helium stars with compact objects. In the studies presented in BK01, we allowed binaries with low-mass helium giants to evolve through DCE and standard SCE, but we had assumed that CE events of helium giants with compact objects lead to mergers, and possibly a gamma-ray burst (e.g., Fryer et al. 1999). However, due to the small mass of helium giant envelope at the onset of CE event ($\sim 1 - 1.5M_{\odot}$), we find that these systems survive the CE events, and form very tight NS-NS binaries (see also footnote in § 2.1.2).

Double neutron stars are formed in various ways through more than 14 different evolutionary channels identified in Table 3. However, the entire population of coalescing NS-NS systems, may be divided into three subgroups.

Group I. This subpopulation consists of non-recycled NS-NS systems, first identified by BK01. These are systems in which none of the two NS ever had a chance of getting recycled through accretion. Our current results for the predicted formation rates and properties of the non-recycled NS-NS systems, have not been affected by the two improvements discussed above. As shown in Table 3, these recently identified non-recycled NS-NS systems are formed via the NSNS:09, NSNS:11 and NSNS:12 channels,

which involve DCE of two low-mass helium giants, which were already allowed in the earlier version of *StarTrack*.

The unique qualitative characteristic of this NS-NS formation path is that both NS have avoided recycling. The NS progenitors have lost both their hydrogen and helium envelopes prior to the two supernovae, so no accretion from winds or Roche-lobe overflow is possible after NS formation. Consequently, these systems are detectable as radio pulsars only for a time ($\sim 10^6$ yr) much shorter than recycled NS-NS pulsar lifetimes ($\sim 10^8 - 10^{10}$ yr in the observed sample). Such short lifetimes are of course consistent with the number of NS-NS binaries detected so far and the absence of any *non-recycled* pulsars among them.

We note that the identification of the formation path for non-recycled NS-NS binaries stems entirely from accounting for the evolution of helium stars and for the possibility of double CE phases, both of which have typically been ignored in previous calculations (with the exception of Fryer et al. 1999, where, however, such events were assumed to lead to mergers).

Group II. This subpopulation consists of tight, short lived binaries with one recycled pulsar. Their merger times are typically ~ 1 Myr or even smaller (see §3.4.5). As shown in Table 3, these new dominant NS-NS systems are formed via the NSNS:01–08, NSNS:10 and NSNS:13 channels, with the common characteristic that the *last* binary interaction is a hyper-critical CE of a low-mass helium giant and the first-born NS.

In Belczynski, Bulik, & Kalogera 2002a we describe in detail the formation of a typical NS-NS binary of group II. The most channel identified as the most efficient for NS-NS formation (NSNS:01) corresponds to the “standard” channel of Fryer et al. (1999). The only difference is an extra CE event which originates from allowing for helium star evolution and without a priori assumptions about the CE outcome. The second most dominant channel, involving two consecutive MT episodes and then two SN explosions, closely resembles our channels: NSNS:02, NSNS:04, NSNS:06, NSNS:10, NSNS:11, NSNS:12. The only difference again remains an extra MT episode from evolved, Roche-lobe-filling helium stars.

The most dramatic effect of the binary evolution updates is reflected in the existence of a whole new population of coalescing NS-NS stars formed in the Group II. In our standard model these channels contribute 50% of the DCO population, and their common characteristic is that the *last* binary interaction is a hyper-critical CE of a low-mass helium giant and the first-born NS. It turns out that the majority of these systems survive the HCE event and form tight NS-NS binaries. Had we not taken into account the radial expansion of low-mass helium-rich giants, the progenitors of this dominant NS-NS population would have evolved without any further MT. Most of them would have still formed NS-NS systems, however, not as tight as after this last CE episode. We have actually examined this alternative and found that about half of them would have formed binaries with merger lifetimes longer than 10^{10} yr. Once again, we see the importance of helium star evolution on DCO population synthesis.

Group III. This subpopulation consists of all the other

NS-NS systems (belonging neither to Group I nor II) formed, through more or less classical channels (Bhattacharya & van den Heuvel 1991). The formation path denoted NSNS:14 corresponds to what is usually considered to be the “standard” NS-NS formation channel (Bhattacharya & van den Heuvel 1991). Since we account for hyper-critical accretion in CE, the formation rate is decreased because some NS (but not all, as assumed by Portegies Zwart & Yungelson 1998 and by Fryer et al. 1999) collapse to BH. Furthermore our treatment of the hyper-critical accretion typically leads to tighter post-CE systems, causing more binaries to merge in CE events, and thus decreases the number of possible NS-NS progenitors.

Group II strongly dominates the population of coalescing NS-NS systems (81%, for standard model calculation) over group III (11%) and I (8%). In general this characteristic is preserved in all, except a few extreme evolutionary models. The discussion of the dependence of the formation rates of the various NS-NS subpopulations on population synthesis model assumptions will be presented in Belczynski et al. 2002a.

3.3.2. Populations of Black Hole Binaries

In general, BH-NS and BH-BH binaries are formed through just a few distinct channels, with a moderate number of MT events (2–3), in contrast to our findings for NS-NS systems.

Helium star evolution, radial expansion and CE phases are much less important for the formation of BH-NS and BH-BH binaries. The reason is that for most of these progenitors the first-born compact object is massive enough that even when helium stars evolve to the giant branch, they do not expand to large radii nor they lead to possible CE evolution (see MT criteria in §2.2.4 and channel BHNS:03 in Table 3). Instead these DCO form most efficiently through channels that closely resemble those NS-NS conventionally thought to be “standard” (Bhattacharya & van den Heuvel 1991; Fryer et al. 1999): evolution is initiated with a phase of non-conservative mass transfer and followed either by a CE phase or the formation of the first compact object (see BHNS:01, BHNS:02, and BHBH:01, BHBH:02).

3.4. Physical Properties of Double Compact Objects

3.4.1. Double Compact Objects Component Masses

Standard Model. In Figure 2, we present the mass distributions of DCO components⁷ for our standard model, with first- and second-born compact objects in the top and bottom panel, respectively.

The shape of the calculated mass distributions can be understood as a convolution of the initial-remnant mass relation for single stars (top panel of Figure 1) with the adopted initial stellar mass function (see eq. 2). Deviations from such a convolution reflect the effects of binary evolution on the compact object masses.

First, we discuss the mass distribution of the second-born compact objects, as they are less affected by binary evolution. This distribution starts at the lowest possible NS mass (allowed by our single star models) of $1.2M_{\odot}$,

⁷Mass distributions of compact objects with white dwarf companions as well as single compact objects (formed both from single star progenitors and from components of disrupted binaries) are presented in Belczynski, Bulik & Kluzniak 2002b.

risks sharply with a peak at $\approx 1.4M_{\odot}$ and then declines down to $\approx 3M_{\odot}$ (the assumed M_{\max}^{NS} for our standard model). This strong peak at low masses is the result of a rather weak dependence of NS mass on ZAMS mass (Figure 1) combined with the steep IMF. Following the initial peak, the distribution becomes flat in the range $\approx 3 - 10M_{\odot}$. This flattening is caused by the balanced effects of a slightly rising initial-remnant mass relation and a declining IMF.

At $\sim 10.5M_{\odot}$ the distribution peaks again, and then rapidly declines. This final peak corresponds to the saturation of BH masses at $\sim 10.5M_{\odot}$ for a wide range of ZAMS masses in the initial-remnant mass relation.

For the model described here, the maximum mass of the second-born compact objects is $\approx 12M_{\odot}$, in excess of the maximum mass of $\approx 11M_{\odot}$ of compact objects formed in single star evolution (Figure 1). Such slightly more massive compact objects are allowed only because of MT episodes involving their progenitors. In some cases they can accrete enough material to significantly increase the core mass (rejuvenation through accretion), and form more massive remnants.

The mass distribution of first-born compact objects shows more prominently the effects of binary evolution, since the compact objects themselves and not just their progenitors might have been affected by mass transfer events. The three basic qualitative features are still present, with an initial peak, a subsequent flattening, and a smaller final peak. However, there are two easily identified differences between the two distributions. First, the initial peak is lower and broader, and second, the peak at high masses shifts to $\approx 13M_{\odot}$, and the maximum compact object mass increases to $\approx 14M_{\odot}$. Both effects are due to accretion onto the first-born compact objects from their non-degenerate companions.

Our standard-model mass distribution of compact objects in coalescing double compact objects peaks at $\sim 1.4M_{\odot}$ for NS and then extends up to $\sim 14M_{\odot}$ for BH. This agrees well with the observed NS masses in binary stars: $1.1 - 1.6M_{\odot}$ (e.g. Thorsett & Chakrabarty 1999) and also with estimated masses of black hole binary candidates: $\sim 3 - 20M_{\odot}$ (for references see §2.1.3). It is important to note that the maximum BH mass of $\sim 14M_{\odot}$ can be increased up to $\approx 20 - 25M_{\odot}$. This can be achieved either by decreasing the wind mass loss rate by factor of 2 (see the bottom panel of Figure 1) and/or by increasing the amount of material accreted by stars in non-conservative MT events.

We can also compare results of our population synthesis calculations to the theoretical compact object mass distributions presented by Fryer & Kalogera (2001, hereafter FK01; their Figures 7 and 8). We find some striking similarities. The single star initial-remnant mass relations are very similar as expected given that our calculation of compact object masses are based on the same core-collapse hydrodynamical calculations (Fryer 1999). FK01 find that in the range of compact object formation 80% of their single star remnants are NS, and the rest are BH. We find that for the standard model of single star evolution 81% of remnants are NS, and 19% are BH.

More importantly, the *shape* of the FK01 CO mass distribution formed in the presence of stellar winds and bi-

nary companions, resembles our distribution, even though FK01 did not use population synthesis. Apart from the qualitative similarities, we also note that our results confirm the findings of FK01 for a continuous mass distributions and the absence of a gap or isolated narrow spike at about $7M_{\odot}$, claimed by Bailyn et al. (1998). Recent observational results also point in the direction of a broader range of BH masses (Froning & Robinson 2001; Orosz et al. 2001). However, there are still two significant differences between our results and those of FK01. One is related to the maximum BH mass (about $10M_{\odot}$ in FK01 compared to our $14M_{\odot}$) and the other to the contribution of BH to the compact object population. Both are linked to a number of binary interactions that are not taken into account by FK01 and have the effect of increasing the masses of compact objects. In our standard-model calculations we find that, in double compact objects, NS and BH represent 65% and 35% of the compact objects, respectively, because of accretion effects. In contrast, for the case in FK01 where effects of stellar winds and binary companions, the contribution of BH actually decreases compared to single star calculations.

Parameter Study. We have explored a large number of population models and have found that the main qualitative features of the mass distributions remain unaffected: the low-mass peak from NS formation and the flat form of the distributions for a wide range of BH masses are present in many different models (e.g., B1, B12, F2, J). Accretion effects and the less prominent peak at higher masses are also clearly seen in almost all of the models.

Nevertheless some dramatic quantitative differences are revealed by a few models. In the case that all wind mass-loss rates are increased by a factor of 2 (G2), the maximum compact object mass turns out to be only $\approx 3.5M_{\odot}$ and therefore such a case appears to be highly unlikely. On the other hand, the model where all wind mass-loss rates are decreased by a factor of 2 (G1) allows for BH masses as high as $\approx 21M_{\odot}$.

Another class of models that show significant quantitative differences from the standard model are those with varying CE efficiencies, especially those with low values. The results for model E1 ($\alpha_{\text{CE}} \times \lambda = 0.1$) are shown in Figure 3. Although the basic shape of the distributions resembles that of the standard model, the second-born compact objects span a much narrower range in mass: $1.15 - 9.7M_{\odot}$ (with most of compact objects formed with mass smaller than $6M_{\odot}$). Low CE efficiency discriminate against tight pre-CE systems, cause a large number of DCO progenitors to merge, and therefore DCO rates to decrease significantly. In particular, the effects appear to be most prominent for BH-BH binaries where massive second-born BH are essentially eliminated. As shown in §3.3 and Table 3 most BH-BH progenitors experience first a non-conservative MT and then a CE episode. For the case of low CE efficiencies, CE survival is favored for rather wide pre-CE systems with donors (stars that initiate the CE episode and progenitors of the second-born compact objects) with low envelope masses. In these cases CE ejection is facilitated, but at the same time lower mass progenitors are favored, leading to a restricted mass range for these second-born compact objects. At the same time the bias in favor of wide pre-CE systems translates to a bias in

favor of progenitors where the first MT episode is initiated late in the evolution of the primary, when the stellar radii are larger and most of the stellar envelope has burnt into a high mass core. This bias clearly favors the formation of higher mass first-born compact objects, leading overall to BH-BH binaries with rather extreme mass ratios.

Given the sensitivity of the DCO mass distribution to the CE efficiencies, it may be possible in the future to discriminate between models based on mass measurements of BH-BH binaries from gravitational-wave detections and data analysis.

3.4.2. Double Compact Objects Orbital Separations

Standard Model. The distribution of DCO over orbital separations at the time of their formation is shown in Figure 4, for our standard model.

The distribution for the whole population (top panel) covers a wide range of values $\sim 0.1 - 100R_\odot$ and is characterized by two distinct peaks. It is evident from the bottom panel that the peak at shorter separations is due to NS-NS binaries and the one at wider is due to BH binaries. Examination of the NS-NS distribution indicates that the majority of NS-NS systems, are formed with very small orbital separations ($< 1R_\odot$), but there is a long tail stretching to much larger orbital separations (even beyond $10R_\odot$). This result is related to our discussion of the main NS-NS formation channels (§3.3). The NS-NS population consists of three distinctive groups (see §3.3.1), which shape the orbital separation distribution. “Classical” NS-NS systems (group III) that contain recycled pulsars have wide separations, mostly in the range $\sim 1 - 10R_\odot$ (where the two observed systems lie). However, NS-NS binaries in which none of the NS ever had a chance of getting recycled (group I) and very tight NS-NS binaries formed via the newly identified channels (group II) actually dominate the produced NS-NS population and produce a strong peak at much lower orbital separations. These differences in orbital separations affect the derived merger times and have important implications for the detection of such systems, which we discuss in §3.5.2.

Typical BH binaries have much wider separations than NS-NS systems (Figure 4). This is a result of the lower (or zero) SN kicks imparted to BH which allows the survival of wider progenitors, typical of the more massive binaries required for the formation of the BH binaries. Note that BH-NS binaries tend to have intermediate size orbits, affected in part by the high kicks imparted to one of the two compact objects.

Parameter Study. The double-peaked shape of the orbital separation distributions found in the standard model persists in a robust way in the majority of the models in our parameter study. The full range of separation values also appears to be robust ($0.1-100 R_\odot$). However, the relative height of the two peaks varies significantly from model to model, primarily because of the varying contribution of different types of systems to the DCO population. The reasons and a discussion of these variations are given in §3.5.1.

Here, we identify a couple of extreme cases: In the models with zero kick velocities (B1) or increased wind mass-loss rates (G2), BH binaries have a very small formation rate relative to NS-NS systems (see also Portegies Zwart &

Yungelson 1998; Fryer et al. 1999), and therefore the NS-NS peak at shorter orbital separations strongly dominates. In contrast, models with low CE efficiencies hamper the formation of DCO in tight orbits and the peak due to BH binaries strongly dominates. In model H2, as expected, the peak at low separations for NS-NS disappears altogether, since no helium-star CE episodes are allowed.

3.4.3. Double Compact Objects Eccentricities

Standard Model. In Figure 5, we present eccentricity distributions of coalescing compact object binaries for our standard model. The values at the time of DCO formation are quite high, $e > 0.1$ for the majority of the population, and of course originate from the fact that the last stage prior to DCO formation typically involves a SN explosion and asymmetric kicks. The fraction of DCO formed in circular orbits is rather small, and occurs when the second compact object is formed through a direct collapse to a BH (BH-BH: $\simeq 2.4\%$ and BH-NS: $\simeq 0.1\%$). Portegies Zwart & Yungelson (1998) and Fryer et al. (1999) have also found that NS-NS population is born with high eccentricities, which is in good agreement with our results.

Apart from the eccentricities at formation, we also examine the distribution at later stages when gravitational radiation has caused the binary orbit to shrink and the gravitational-wave frequency has increased to $\simeq 40$ Hz, the lower end of the LIGO I band. So far DCO have been assumed to be circular for purposes of gravitational-wave detection and data analysis. We examine whether our model population satisfies this assumption due to angular momentum losses and circularization. We use the dependence of orbital separation on eccentricity due to gravitational-wave emission as derived by Peters (1964):

$$A(e) = \frac{c_0 e^{12/19}}{(1 - e^2)} \left[1 + \frac{121}{304} e^2 \right]^{870/2299}, \quad (18)$$

where c_0 is given in equation 14 and depends on the orbital separations and eccentricities at DCO formation. We use our results for the masses to calculate first the orbital separation at 40 Hz and the corresponding frequency. The resulting distribution is shown in Figure 5 (solid line). It is clear that by the time these coalescing DCO enter the LIGO I band, the eccentricities are small enough ($e < 0.0001$) that the assumption of circular orbits is well justified.

It is interesting to note that, although the eccentricity distribution at birth is single-peaked, the distribution at later stages becomes double-peaked. This is a direct result of the double-peaked form of the orbital separation distribution. In more detail, the peak at lowest eccentricities is populated by the heavier BH binaries and the peak at somewhat higher eccentricities by NS-NS binaries. The distinction is related to the weaker effects of gravitational-wave emission for the less massive systems.

Parameter Study. The shape and range of typical values for the orbital eccentricities appear to be quite robust. Differences becomes noticeable only in models of varying kick-magnitude distributions. As expected, the typical eccentricities at formation decrease with a decreasing average kick magnitude.

The variations in the shape and position of the eccentricity peaks for later stages are more prominent and closely follow the corresponding variations in the distributions over orbital separations. Nevertheless, the eccentricities at 40 Hz remain below 10^{-3} for all the models we have examined.

3.4.4. Double Compact Objects Center of Mass Velocities

Standard Model. Binaries are expected to acquire systemic (center-of-mass) velocities after core-collapse events because of the combined effects of mass loss and SN kicks imparted to the compact remnants. Understanding of these velocities is crucial in studies of dynamical evolution of these populations, and their kinematic properties and spatial distributions with respect to host galaxies. The distributions of center-of-mass velocities after the first and second core-collapse events are shown in Figures 6 and 7, respectively. Top panels on both figures show the distribution for the whole DCO population, and bottom panels show the distributions separately for each of the DCO groups.

It is evident that there are major differences between the two plots. The distribution after the first core-collapse event (V_1) shows a well defined narrow peak at low velocities ($\sim 25 \text{ km s}^{-1}$) and a slowly decaying tail at higher velocities. After the formation of the second compact object velocities (V_2) populate a much broader peak positioned at high magnitudes ($\sim 200 \text{ km s}^{-1}$) with a velocity tail reaching to very high velocities ($> 600 \text{ km s}^{-1}$). Moreover, in these distributions a narrow spike at 0 km s^{-1} is also identified.

All these characteristics can be naturally explained by the different binary orbital properties of binaries at the time of the first and the second compact object formation. For the majority of DCO progenitors, the first core-collapse event happens when the binary orbit is still wide, accommodating two massive stars and is affected primarily by mass loss through winds and non-conservative mass transfer events. The typical orbital velocities in these pre-collapse systems are $\sim 10 - 50 \text{ km s}^{-1}$ and it is mostly these orbital velocities that determine the typical post-collapse systemic velocities of bound systems (Kalogera 1996). For Maxwellian kick magnitude distributions an upper and lower limit on the systemic velocity can be derived analytically and it is found to be independent of the average kick magnitude (depends only on the stellar masses and the pre-collapse relative orbital velocity; see Kalogera 1996). As a secondary effect, within the range of values defined by these two limits, systems tend to acquire higher systemic velocities when higher kicks are imparted. A smaller fraction of DCO progenitors experience a CE phase prior to the first core-collapse event, and have much tighter orbits (orbital velocities of order $\sim 100 \text{ km s}^{-1}$), leading to higher systemic velocities. The more subtle influence of the average kick magnitude is evident when looking at the distributions for each DCO class, where NS-NS progenitors are slightly shifted to higher and BH binaries to lower systemic velocities (NS-NS progenitors tend to be lighter than BH-BH progenitors).

At the time of the second SN explosion, the population of compact object binary progenitors is dominated by tight

binaries with relative orbital velocities in the low hundreds. The result is a strong, broad peak at $100 - 300 \text{ km s}^{-1}$ with a tail to higher velocities (Figure 7). Systems with lower systemic velocities do form, but the majority of them are so wide that their merger times exceed the Hubble time. Another noticeable difference from Figure 6 is that the BH-NS population now closely follows the NS-NS population. This is understood as both the pre-collapse orbital characteristics and the typical kick magnitudes are similar for these two populations at the second compact object formation, since in the majority of BH-NS systems the NS is formed second. It is evident that typically BH-BH binaries acquire the lowest systemic velocities. This is a result of three combined effects: they are formed from wider progenitors (§ 3.4.2), they are heavier systems, and some BH are formed via direct collapse and hence do not acquire any kick. Strikingly, in both Figures 6 and 7, there is a prominent spike at zero systemic velocity, which is populated by BH-BH systems where both BH were formed via direct, assumed to be symmetric collapse. We note that, although these systems tend to be wider than NS-NS, they still merge within a Hubble time because of the higher masses, hence stronger gravitational radiation involved.

It is useful to note one other implication of the small systemic velocities after the first core-collapse event. These combined with the fact that the time between the two collapse events is much shorter than typical coalescence times, implies that it is the systemic velocities after the second collapse (along with the merger times) that determine the spatial distributions of DCO merger sites with respect to host galaxies.

Portegies Zwart & Yungelson (1998) presented results on NS-NS systemic velocities, and Fryer et al. (1999) calculated systemic velocities for both NS-NS and BH-NS binaries. Comparison with our results shows overall good agreement; both Portegies Zwart & Yungelson (1998) and Fryer et al. (1999) found that most systems acquire systemic velocities of the order of $\sim 200 - 300 \text{ km s}^{-1}$, with some binaries being accelerated to much higher velocities ($\sim 500 - 1000 \text{ km s}^{-1}$).

Parameter Study. The distribution of systemic velocities after the first core-collapse event is found to be very robust in our parameter study. The most clear, but not big, changes in the distribution shape are visible in models which affect the pre-SN orbital separations, e.g. in models E1 and F2. For these models, the distribution starts with an initial peak, as for the standard model, however the high velocity tail is depleted at velocities below $100 - 150 \text{ km s}^{-1}$. All of DCO progenitors experience either CE phase or MT event prior to the first SN explosion. Decreasing the CE efficiency (model E1) or increasing the fraction of mass accreted by companions in MT events (model F2) lead to a decrease in post-CE or post-MT separations. Therefore, at the time of the first SN explosion, progenitors have higher orbital velocities, and DCO progenitors in models E1 and F2 end up with higher systemic velocities than in the standard model, depleting the distribution of low velocity values. Some small changes are also seen with kick magnitude variations. For very small kicks, the high velocity tail of the standard model distribution disappears, whereas, for very high kicks, many more systems are disrupted, but most of the ones that survive

the collapse, end up with somewhat higher systemic velocities. As a result, the low velocity peak of the distribution is depleted and the tail extends to higher velocities.

Similarly, the qualitative features of the distributions after the second compact object formation are robust, with an exception for the spike at zero velocity, the presence of which depends on the contribution of BH-BH binaries to the DCO population (e.g., models B1, B6, B13, D2, F2, J, and the extreme case of G2 where essentially no BH-BH binaries are formed). For a few models, we find some significant differences, but are all explained by the relative contribution of the various DCO groups. For example, for very high kicks (model B12) and in the absence of helium-star CE phases (model H2), the formation rate of coalescing NS-NS is so small that the velocity distribution is dominated by BH-BH binaries, and in particular those which do not receive a kick (i.e., the zero-velocity spike becomes most dominant). The few surviving NS binaries populate a much broader range of systemic velocities with low normalization and a roughly flat tail out to hundreds of km s^{-1} .

3.4.5. Double Compact Objects Merger Times

Standard Model. The distributions of merger times (see eq. 14) of coalescing DCO are shown in Figure 8, for our standard model. The double-peaked form is due to the two main populations of NS-NS systems and BH binaries and their double-peaked distributions of orbital separations. As already mentioned the NS-NS population is dominated by tight binaries formed through channels involving MT episodes from helium stars. These tight orbits imply very short merger times with a peak at $\sim 0.3 \text{ Myr}$. Despite their higher masses BH-NS and BH-BH binaries are found to have merger times typical of $\sim 1 \text{ Gyr}$, driven by their wider orbits and the stronger dependence of merger time on separation. Merger times also decrease with increasing initial eccentricities, leading to a stronger separation of the two peaks, since NS-NS binaries tend to have not only tighter orbits, but also higher eccentricities.

In the bottom panel of Figure 8, we present the merger times of three different populations of coalescing NS-NS binaries (see §3.3.1): group I of tight, non-recycled NS-NS binaries; group II of tight binaries formed through the newly identified channels; and group III of NS-NS formed through “classical” channels. It is evident that the large relative contribution of the tight NS-NS binaries drives the typical NS-NS merger times down to values close or below 1 Myr , whereas the “classical” NS-NS have merger times typical of the BH binaries. The identification of these short-lived binaries has important implications for the detectability of coalescing NS-NS binaries (see §3.5.2).

Both, Portegies Zwart & Yungelson (1998) and Fryer et al. (1999), presented merger time distributions of NS-NS binaries. They obtained typical times much longer than ours, close to $100\text{--}1000 \text{ Myr}$. This discrepancy originates from the newly identified short-lived NS-NS systems. However, our classical population of NS-NS binaries have, as expected, merger times comparable to these found in

these two earlier studies.

Parameter Study. Unlike all other binary properties we have examined, the qualitative characteristics of the merger-time distributions appear to be rather sensitive to a number of model parameters. This is understood in terms of the strong dependence of merger times on initial separations and eccentricities, and, although their distributions change only slightly with model parameters, the corresponding change of merger time distributions is quite dramatic. In Figure 9, we show three of the most different DCO merger time distributions from models with somewhat extreme assumptions.

In the top panel of Figure 9 (model with zero kicks, B1), the DCO population is dominated by the NS-NS binaries, causing at first a sharp rise followed by a slow decline at longer merger times (compare to the middle panel of Figure 7). The flattening of the distribution at $10^2\text{--}10^4 \text{ Myr}$ is due to the small contribution of BH-NS and BH-BH systems to the DCO population in this model. In the model shown in the middle panel (model F2), all dynamically stable MT episodes are assumed to be conservative. The distribution is rather flat over a wide range of merger times and this is mainly a result of the assumption of conservative MT and the wider orbits that form as a consequence. In the bottom panel, we show results from a model with low CE efficiency (model E1). It is evident that the distribution is depleted of short merger times. In contrast to the previous two models, the population is dominated by BH-NS and BH-BH systems, which have in general wider initial separations, and thus longer merger times than NS-NS binaries. Model H2 (no helium-star CE phases) shows a very similar behavior with the peak at short merger times disappearing.

Other models lead to the double-peaked distributions similar to our standard-model results. The range of values remains unchanged, but the relative strength of the two peaks vary slightly from model to model following the variations of the dominant classes within the DCO population.

3.5. Results on Double Compact Object Coalescence Rates

3.5.1. Galactic Coalescence Rates of Double Compact Objects

The calculated DCO coalescence rates have been calibrated using the latest Type II SN empirical rates normalized to our Galaxy⁸ (Cappellaro, Evans, & Turatto 1999). In Table 4 coalescence rates are given for all the models in our study for each of the DCO classes as well as for the whole population. For our standard model (A), rates were calculated from a very large number of primordial binaries (3×10^7) and sub-samples of DCO formed from each of 10^6 -binaries runs were used to examine and ensure the statistical accuracy of the results (see §3.2). All other rates are based on models with $N \geq 10^6$ primordial binaries. For each model, we have also evolved an equal number of single stars, except for models K1-2, for which

⁸Following van der Kruit (1987) we have adopted a value of $2 \times 10^{10} L_{\odot}$ for the blue luminosity of the Galaxy, the value used in several other studies, e.g., Phinney (1991) or Portegies Zwart & Yungelson (1998). Some recent results point to a value lower by a factor of $\simeq 2$ (see discussion in Kalogera et al. 2001, and references therein). Had we adopted this lower value, all our coalescence rates would also be decreased by the same factor of $\simeq 2$.

we appropriately adjusted the contribution of single stars based on the assumed binary fraction.

In Figure 10, we illustrate the rate dependence on the assumed kick velocity distribution. There is an overall decrease of rates with increasing kick velocity for every population of coalescing double compact objects, as the disruption probability for pre-collapse systems increases with higher kick magnitudes. It is worth noting though that at small kicks (from zero to average magnitudes of $\sim 30 \text{ km s}^{-1}$) rates are found to increase. This is due to the importance of kicks in creating tight binaries with merger times shorter than a Hubble time (see Fryer & Kalogera 1997 and Fryer et al. 1999 in the NS-NS case). Rates remain roughly constant for $\sigma = 20 - 50 \text{ km s}^{-1}$, as the two effects balance one another. It is also notable that the rate decrease is steeper for NS-NS binaries, and progressively flattens for BH-NS and BH-BH binaries. This is a result of the lower kick magnitudes assumed to be imparted to BH. For very high kick magnitudes (Maxwellians with $\sigma > 400 \text{ km s}^{-1}$), BH-BH systems start dominating the population, as most of the NS-NS progenitors get disrupted. These results are in qualitative agreement with previous studies (e.g., Lipunov et al. 1997; Portegies Zwart & Yungelson 1998; Fryer et al. 1999). In Figure 10, we also plot the rates from our standard model (kicks similar to the results by Cordes & Chernoff 1998) and the model B13 with “Paczynski-like” kicks. It is evident that, despite the very different shape of these distributions, they closely correspond to Maxwellian kicks with $\sigma \simeq 240 \text{ km s}^{-1}$ and $\sigma \simeq 150 \text{ km s}^{-1}$, respectively. This result once again indicates that the kick distributions are narrowly “filtered” by DCO binary properties: only binaries receiving kicks similar to their orbital velocities have a good SN survival chance (Kalogera 1996). The match between these two models and the specific σ -values of the Maxwellians indicates that the normalizations in the velocity range of interest happen to be very similar and the shape of the distributions outside this range becomes irrelevant.

The effects of hyper-critical accretion combined with the assumed maximum NS mass can be understood on the basis of the results of models C and D1-2. We find that hyper-critical accretion in CE phases not only increases the mass of the inspiraling compact objects and can convert NS to BH, but also leads to somewhat wider post-CE systems because part of the envelope is accreted and does not need to be expelled at the expense of orbital energy. In model C, we do not allow for any hyper-critical accretion and we find that the rate of NS-NS and BH-NS systems decreases whereas the rate BH-BH binaries remains unaffected. This combination indicates that it is the effect on the orbital period (increased rate of post-CE mergers) that dominates over the reduction of NS conversions to BH. BH-BH systems originate from wider progenitors and therefore are not much affected. The reduction in NS conversions to BH turns out to be unimportant because the assumed maximum NS mass is rather high and the rate of conversions is low in the standard model (only 5% of all NS entering CE phases). In contrast, when the maximum NS mass is reduced to $2 M_{\odot}$ and $1.5 M_{\odot}$ (models D1 and D2), 34% and 80% respectively of NS entering CE phases collapse into BH. In these two models there is also a clear decrease in the rate of NS binaries and increase

of the BH-BH coalescence rates, whereas the total DCO coalescence rates remain essentially constant (within our statistical accuracy, see § 3.2).

The effects of varying the effective CE efficiency (models E1-3) are qualitatively similar to not allowing for hyper-critical accretion (model C). Coalescence rates tend to decrease with decreasing CE efficiency because of an increased rate of CE mergers. The main difference with model C is that the BH-BH rates are altered here. This is because varying the CE efficiency by factors of 2 or more affects post-CE binary separations much more than decreasing envelope masses of an ejected envelope by a few tenths of a solar mass in model C.

In models F1-2 and L1-2, we vary the parameters governing mass loss in non-conservative MT episodes, and in particular in model F2, we obtain results for conservative mass transfer. Most of the NS-NS progenitor systems ($\sim 75\%$) start their mass transfer history with a non-conservative exchange, and therefore their coalescence rates might be altered. Also for many other compact binary progenitors, non-conservative mass transfer phases may take place, particularly at the early stages of binary evolution, when the primary expands and evolves toward the red giant branch while its companion is still on the main sequence. However, non-conservative mass transfer phases do not drastically change the orbital separation, so we find that the overall coalescence rates do not change by much. Comparison to our standard model shows a depletion in coalescing BH-BH systems for both F1-2 and L1-2 models, and also moderate decrease of NS-NS binaries for the F1 and L2 models. Coalescence rates of BH-NS binaries are not significantly altered. The similarities of the results come from the same effect that the fact that the F and L model parameters affect post-MT orbital separation in a similar way. In models F, we vary f_a , the amount of material which is accreted onto the companion star, while in models L, we change the specific angular momentum j of the material lost from system during MT ($1.0 - f_a$). Both an increase of f_a (F2) and decrease of j (L1) lead to an increase of the final post-MT orbital separations. On the other hand, both a decrease of f_a (F1) and increase of j (L2) lead to a decrease of the final post-MT separations. (see eq. 8 and eq. 9, or original study of Podsiadlowski et al. 1992). Note, that orbital separations also depend on the mass ratios, but here we only discuss the changes relative to the standard model. It turns out that these orbital separation changes have different effects on different DCO populations. For NS-NS progenitors, pre-MT orbits are already relatively tight, so in models F1 and L2 (F2 and L1) the NS-NS rate decreases (increases) as the frequency of mergers increases (decreases). Progenitors of BH-BH systems are more massive and generally have wider orbits at the onset of MT episodes compared to the progenitors of NS-NS binaries. Given the decreased post-MT separations of model F1 and L2, the BH-BH rate drops as in the case of NS-NS systems and for the same reasons. However, for the increased post-MT separations of model F2 and L1, the BH-BH rate drops as well, this time due to the fact that many final BH-BH binaries are not tight enough to coalesce within the Hubble time.

Variation of wind mass loss rates (models G1 and G2) affects more strongly the rates of BH binaries, which de-

crease with stronger mass loss. The extreme case of wind losses even stronger than in our standard model entirely eliminates the BH-BH population, but increases the overall DCO rate, mainly because survival through CE phases and SN events is facilitated (lower-mass envelopes).

As we pointed out in §2.1.2 (see also Belczynski & Kalogera 2001), the maximum mass of helium stars that develop convective envelope is somewhat uncertain (thought to lie within the range of $3.5 - 4.5 M_{\odot}$), and therefore we treat it as a model parameter. We find that reducing this value to $M_{\text{conv}} = 4.0 M_{\odot}$ (model H1) results in NS-NS coalescence rate decreased by 30%. This is expected since many of the NS-NS formation channels (see Table 3) involve CE evolution of helium stars, which is aborted in the absence of convective envelopes. If we further eliminate the possibility of CE evolution even for low-mass helium stars (model H2), the NS-NS coalescence rate drops to 0.9 Myr^{-1} .

Although it is not thought to be relevant for our Galaxy, we examine one model where star formation is assumed to be burst-like and to have occurred 10 Gyr ago (model I). We find that all coalescence rates are increased because a larger fraction of them had enough time to evolve and have total lifetimes shorter than 10 Gyr.

As expected, a flatter IMF (model J) favors the formation of NS and even more of BH, so the contribution of BH-BH and BH-NS systems increases as the overall DCO coalescence rate increases as well.

Varying the binary fraction affects the overall normalization of our population synthesis models. Binary systems mostly contribute to type Ib/c SN and therefore an increased binary fraction decreases the absolute number of Type II SN in the model and, for an assumed Type II SN normalization (based on the empirical estimates), leads to an increase of the coalescence rates.

In model N, we see that rates of systems containing BH are similar to those of the standard model. However, the rates of NS-NS are much depleted. This is due to the fact, that in model N, with no helium star radial expansion, the NS-NS progenitors avoid the last CE episode of standard model formation channels. Therefore, many NS-NS systems of model N are not tight enough to merge within the Hubble time.

In models M, where we used different distributions for the initial binary mass ratios, the total DCO coalescence rates are reduced or increased, depending on whether extreme mass ratios (small q values) are favored or not. In model M1 the MT events are generally dynamically unstable, leading very often to mergers long before compact object systems form.

Evolution of model O influences only systems containing a BH, as in this model we have allowed for BH formation only through partial fall back. In the standard model, some BH were formed through a direct collapse of a massive star, and no kick was imparted to such BH nor any material was lost from the binaries. Extending the influence of BH formation through partial fall back increases the overall probability that binaries are disrupted. Thus coalescence rates of BH-NS and BH-BH binaries in model O are lower.

3.5.2. Rate Increase Factors for Empirical Estimates of NS-NS Coalescence

Coalescence rate estimates based on the observed sample of close NS-NS systems need to account for all possible observational biases acting against their detection. Systems with two NS are discovered as binary pulsars. The two coalescing systems that have been observed in the Galactic Observed sample of NS-NS systems contain recycled NS with long pulsar lifetimes ($\sim 10^9$ yr) and long merger times ($> 10^8$ yr), and empirical estimates are obtained under the assumption that the observed systems are representative of the Galactic population (Kalogera et al. 2001).

As emphasized in our earlier work (Belczynski & Kalogera 2001), empirical coalescence rate estimates could be increased in light of the new short-lived NS-NS sub-populations identified in studies of their formation. *Rate-increase factors* can be calculated to account for the populations of (i) non-recycled NS-NS, and (ii) tight NS-NS binaries with very short merger times formed through the new formation channels identified in the present study. Because of their highly reduced lifetimes (pulsar and merger), the detection efficiency for these NS-NS sub-groups is practically diminished (drops by ~ 3 orders of magnitude).

In Table 5, we present Galactic coalescence rates of: non-recycled NS-NS, tight NS-NS binaries with merger times shorter than 1 Myr, and the complete NS-NS population. In the last column of Table 5 we give the correction factors for empirical coalescence rates calculated from:

$$\frac{\mathcal{R}}{\mathcal{R} - (\mathcal{R}_{\text{nr}} + \mathcal{R}_{\text{tight}})}, \quad (19)$$

where \mathcal{R} is the rate of all coalescing NS-NS binaries, \mathcal{R}_{nr} is the rate of coalescing non-recycled NS-NS (group I), $\mathcal{R}_{\text{tight}}$ is the rate of systems (of group II and III) with merger times smaller than 1 Myr. These correction factors imply an increase of the NS-NS rate estimated empirically based on the observed NS-NS with long pulsar and merger lifetimes.

It is evident from Table 5 that systems formed through the new “helium-star” channels (group I and II) contribute the most to the correction factors. Our standard model prediction is that empirical rates may be increased by a factor of 2.5 to account for short-lived NS-NS pulsar systems. Although the correction factors change significantly for a few of the models, i.e., from 1.4 to 6.1 for models with different CE efficiency (E1–3), they remain roughly constant at ~ 2.5 for most of the models in our parameter study. Only for the nonphysical model N, with no helium star radial evolution, the correction factor is found as expected to be 1.0. Note that even for model H2 (no helium-star CE evolution) there is a small fraction of short-lived systems (primarily due to kicks instead of CE orbital shrinkage) and the correction factor is 1.1. In model N no correction is needed, as in this model we do not form any NS-NS binaries in groups I nor II, and both these groups are primarily responsible for the increase factors (see also footnote in §2.1.2).

For our correction-factor estimates we have conservatively assumed (i) that a recycled NS is formed in *all* NS-NS binaries in which the first-born NS had an opportunity to interact with its non-degenerate companion, even

though this may not be true (given our limited understanding of recycling we cannot be certain). We characterize non-recycled NS-NS only systems that evolved through a double CE phase involving two helium stars (channels NSNS:09, NSNS:11, and NSNS:12); (ii) that systems with merger times longer than 1 Myr can be detected with the same efficiency as much longer lived binaries, even though in reality there is a continuum, given the continuous distribution of merger times (Figure 7). Because of these two assumptions we should consider the derived upwards correction factors to be rather conservative and represent more of lower limits than rough estimates.

3.5.3. Predicted Supernova and Star Formation Rates

Cappellaro et al. (1999) estimated the rates of Type II SN and Type Ib/c SN to be 0.86 ± 0.35 SNu and 0.14 ± 0.07 SNu for Sbc-d galaxies, where 1 SNu corresponds to one SN per 100 yr and the estimates are normalized to a blue luminosity of $10^{10} L_{\odot}^B$. For an estimated Galactic blue luminosity of about $L_{\odot}^B = 2 \times 10^{10} L_{\odot}$ (van der Kruit 1987; although see footnote in § 3.5.1), we obtain 1.72 and 0.28 SNu for Type II and Ib/c SN, respectively. The ratio of Type II to Type Ib/c SN turns out to be quite uncertain: 6.1 ± 4.0 . Note that this ratio is independent of the assumed blue luminosity for our Galaxy.

In our population synthesis calculations we keep track of all SN events. We use Type II events to normalize our models and then combine them with the Type Ib/c rates to derive the model-predicted II-to-Ib/c ratios. We find them to lie in the range 1.8 – 3.7, for all the models in our parameter study, with the standard model yielding a ratio of 2.6. Although our predicted ratio values are consistent with the empirical estimates within the associated errors, we note that the theoretical values tend to be systematically lower than the empirical estimates, implying that our Ib/c rates are rather high. In retrospect, this is actually expected given some of the assumptions in the MT events. We note that in dynamically stable and unstable MT episodes, we assume that the donors are always stripped of their envelopes. However, it is not at all clear that this is a realistic assumption in small cases and it is quite possible that a small fraction of the H-rich envelope remains with the post-MT/CE donors. Since our classification of SN events as type Ib/c is based on the exploding stars having lost their H-rich and/or He-rich envelopes, it is possible that we are overestimating the Ib/c events because of this assumption. We note, however, that all our models remain consistent with the empirical rates within the estimated errors.

Another explanation for the possible overabundance of Type Ib/c SN in population synthesis model has been provided by De Donder & Vanbeveren (1998). Our results are consistent with their findings of II-to-Ib/c ratios of 2-3. The explanation they offered was related to possible variations of massive binary formation in galaxies over a range of morphological types and to the empirical estimates representing an average over many galaxies and not being appropriate for our Galaxy. However, in their study De Donder & Vanbeveren (1998) considered the results obtained by (Cappellaro et al. 1993a,b) that were available at the time. In contrast, the most recent study of empirical SN rates (Cappellaro et al. 1999) accounts

for different morphological types of galaxies, possibly implying that the MT assumptions (common to our and the De Donder & Vanbeveren 1998 study) may be primarily responsible for the calculated SN small rate ratios.

Galactic SFR have been estimated to lie in somewhat broad ranges of $1 - 3 M_{\odot} \text{yr}^{-1}$ (Blitz 1997; Lacey & Fall 1985) and $\sim 1 - 10 M_{\odot} \text{yr}^{-1}$ (Gilmore 2001). We use the calibration to the Type II SN rate by Cappellaro et al. (1999) with the adopted blue luminosity of our Galaxy: $2 \times 10^{10} L_{\odot}$ (van der Kruit 1987) to calculate the Galactic SFR corresponding to our models. To do so we have to make an assumption about the extension of the IMF down to $0.08 M_{\odot}$. If we assume that the IMF continues as a steep power-law down to the hydrogen-burning mass limit, we obtain values in the range $7 - 28 M_{\odot} \text{yr}^{-1}$, which is clearly significantly higher than current estimates for the Galactic SFR. Based on the results of Scalo (1986, see also Kroupa, Tout, & Gilmore 1993), the IMF is thought to flatten for masses below about $1.0 M_{\odot}$. With the assumed flattened IMF of Kroupa et al. (1993), we obtain much lower SFR values in the range of $3 - 9 M_{\odot} \text{yr}^{-1}$, with the standard model prediction of $\sim 6 M_{\odot} \text{yr}^{-1}$. Moreover, had we adopted the lower, by a factor of two, blue luminosity of our Galaxy (see Kalogera et al. 2001, and references therein) the predicted SFR would decrease (by the factor of two) even further. We note the good agreement of the Galactic SFR estimates with our predictions for a flattened IMF.

3.5.4. Comparison With Other Studies

In § 3.4 we compared our results for the physical properties of DCO populations to those of earlier studies wherever possible. In this subsection we explicitly focus on such a comparison based on results for coalescence rates from the following studies: Lipunov et al. (1997), Portegies Zwart & Yungelson (1998, hereafter PZY), De Donder & Vanbeveren (1998, hereafter DDV), Fryer et al. (1999, hereafter FWH), and Nelemans et al. 2001b.

Lipunov et al. (1997) focused their study on the effect of SN kicks on coalescence rates of double compact objects. Their calculations showed that, in general, the rates decrease approximately exponentially with increasing kick magnitude. This finding is in very good agreement with our calculations (see § 3.5.1 and Figure 4). We also see that the behavior of *relative* coalescence rates of NS-NS to BH-NS binaries is quite similar to what we obtain here. In both studies, the ratio of rates (NS-NS to BH-NS) decreases with increasing average kick velocity. However, the absolute coalescence rates differ and this is easily understood as a result of different population synthesis assumptions, important for the calculation of coalescence rates. In particular, Lipunov et al. (1997) use quite different compact object formation scenarios, as well as a different IMF.

PZY studied the formation and evolution of NS-NS and BH-NS binaries and included a limited parameter study. Nelemans et al. (2001b) calculated populations of Galactic binaries with white dwarfs, NS, and BH, and estimated the low-frequency gravitational-wave emission of these binaries. They used a population synthesis code similar to that of PZY, with few modifications concerning BH formation. Although, many of the population synthesis assumptions differ, we find some similarities in the results.

In general, rates of NS-NS binaries are higher than those of the BH-NS systems. However, in all PZY models NS-NS dominate over BH-NS binaries, which is not true for all of our models mainly because of our more extensive parameter study. Moreover, on average the rates obtained by PZY are smaller than ours, but for some comparable models they differ only by factors of a few. This is due to the newly identified population of NS-NS binaries, as well as to the other differences in model assumptions. PZY note that due to hyper-critical accretion onto NS in CE phases, the population of BH-NS may dominate over NS-NS systems. Although, they do not perform actual calculations of hyper-critical accretion events (they assume that NS always collapse to BH), their results are in agreement with ours, provided that the maximum NS mass is rather low (smaller than $2.0 M_{\odot}$, see rates of models D1 and D2 in Table 4). The predicted BH-BH coalescence rates are diminishingly small in both studies (BH-BH binaries form but in very wide orbits with merger times longer than a Hubble time). This is the combined result of a number of factors: in these two studies BH are assumed to form (i) symmetrically and no birth kicks are taken into account, and (ii) only from progenitor stars more massive than $40 M_{\odot}$, which biases the population to lower frequencies and wider orbits.

With respect to the DDV study, we note the difference between formation rates that correspond to the entire population and coalescence rates that correspond to the subgroup with coalescence times shorter than a Hubble time. DDV reported formation rates and hence a direct comparison with their results is difficult. Overall their formation rates are very high (not only compared to our results but also all the other population studies): ~ 400 NS-NS, ~ 2000 BH-NS and ~ 140000 BH-BH systems per Myr in Galaxy. DDV comment that their BH-BH formation rate is surprisingly high. One reason may be their calibration method based on an assumed massive star formation rate of one massive star per year. This does not easily transform into a star formation rate as used in this work and consequently makes the comparison very difficult.

FHW focused their work to the study of gamma-ray burst progenitors and among them NS-NS and BH-NS binaries. They performed quite an extensive parameter study and calculated coalescence rates for all their models. Once again, we note the very similar dependence of their rates and ours on the average kick magnitude. One striking difference comes with the very wide ranges of their predicted rates (e.g., their 4 orders of magnitude change of NS-NS coalescence rate compared to about 2 orders of magnitude found here). The enormous spread of rates in the FHW work comes from the fact, that in one of their models they, non-physically, increased (by factor of four) the maximum stellar radii to explore the uncertainty related to radius determination in evolved stars. Such a change significantly affects the evolution of many binaries, since the stellar radius is a crucial quantity in judging on the occurrence or non-occurrence of one of the most important binary processes: MT events. The radii we calculate for stars come from the stellar evolution models, and they depend on the star mass, its evolutionary stage, and its composition, and they are not altered in any nonphysical way. However, the FHW models of varied radii show the

sensitivity of the results of population synthesis to this parameter, which is not very well constrained by stellar evolution models.

The results on coalescing compact object binary rates are in good qualitative agreement with previous theoretical predictions. Although we have noted some systematic differences we are able to attribute them to the different population synthesis model assumptions, as well as to the effects of the newly identified populations of NS-NS binaries.

4. DISCUSSION

Close binaries of NS and BH have attracted an increased interest in recent years primarily because of their connection to gravitational-wave detection and possibly to gamma-ray burst progenitors. Here we focus the discussion of our results in the context of gravitational-wave detection by the upcoming ground-based interferometers (e.g., LIGO) and the prospects of detecting inspiraling DCO. An analysis of these and other populations in connection to gamma-ray bursts is presented in Belczynski, Bulik & Rudak 2002c and Perna & Belczynski 2002.

Our motivation in initiating this study was to examine DCO populations in view of some developments in the understanding of CE evolution, particularly the possibility of double CE ejection (suggested by Brown 1995) and hyper-critical accretion (suggested and quantified by Chevalier 1989, 1993; Brown 1995; Bethe & Brown 1998, and in the present study), and the evolution of low-mass helium stars. Some, although not all, of these possibilities have been explored in some of the earlier population synthesis studies, but not in a consistent and equally detailed way (mostly some extreme cases have been examined; for example, either hyper-critical accretion has been ignored or all NS entering a CE have been assumed to collapse to BH). Our goal is primarily two-fold: (i) to examine the predicted rates for various DCO classes, focusing mainly on the relative formation frequencies and their behavior with a large number of model parameters, and (ii) to examine in detail the physical properties of the various populations, the origin of their characteristics, and the links to certain key evolutionary effects or phases, and to identify the most robust of the qualitative features in the distributions of binary properties.

In the course of our investigation we came across a number of new formation channels leading to rather efficient formation of NS-NS binaries. Apart from an increase in the predicted rates, examination of their properties revealed that in their majority these NS-NS binaries form a very distinctive class with tight orbits and short merger timescales (i.e., lifetimes). The common thread connecting all these new formation paths is the evolution of low-mass helium stars and the implications of the fact that they can develop partially or fully convective envelopes. We find that a large number of MT episodes initiated by these evolved stars lead to high survival rate through a CE phase and the production of very tight binaries, which in turn have very high survival probability through the second core-collapse event. Further, following the basic argument made by Brown (1995) we have allowed for the possibility of two giant stars (He-rich more relevant to efficient DCO formation, but also H-rich) involved in the

dynamically unstable MT to eject the two combined common envelopes. It is these possibilities that lead to qualitative changes in the DCO population characteristics, which have been discussed above.

It is important to acknowledge that the viability of these new formation channels has not been examined with detailed evolutionary and hydrodynamical calculations. Despite the difficulties of fully understanding the details of CE phases, questions such as: “are DCE events realistic?”, “can evolved helium stars survive a CE phase?”, and “under what conditions?”, are currently traceable (model H2 corresponds to the case of the answers to the above questions being no for helium stars). It seems that such investigations are necessary before we can include these new channels as part of what is considered “standard” ways of forming DCO. Nevertheless it is interesting to examine the implications of such evolutionary phases (see also Fryer et al. 1999; Nelemans et al. 2001a).

In the context of gravitational-wave detection from inspiraling NS-NS binaries, these relatively short-lived systems imply that empirical rates derived based on the observed sample (with much longer lifetimes) should possibly be raised by factors of 2-3 typically. The reason is that they correspond to a Galactic NS-NS population that is not represented in the observed binary pulsar sample but would very well contribute to inspiral events. Using the results of Kalogera et al. (2001) for the empirical NS-NS coalescence rate, we find that their *most optimistic* prediction for the LIGO I detection rate could be raised to at least 1 event per 2 years, and their *most pessimistic* LIGO II detection rate could be raised to 5 events per year or even higher.

In Table 6 and Table 7 we present our theoretical predictions of detection rates of different binary merger types for LIGO I and LIGO II, respectively. These detection rates correspond to our coalescence rates of double compact objects calculated with the *StarTrack* population synthesis program. Using the extragalactic extrapolation of Kalogera et al. (2001) and the maximum sensitivity distances of LIGO I and LIGO II for a given binary merger type (see Kalogera & Belczynski 2001), we converted our Galactic coalescence rates to detection rates. We find that the LIGO I detection rates are quite low with a *maximum* total rate of a couple events per year and with rates significantly below 1 event per year for many models. However, we find that the prospects for double compact object inspiral detection are very encouraging for LIGO II, for which we predict at least $\simeq 10$ detections per year, even in the most pessimistic case. Moreover, for LIGO II, the total detection rate of compact object binaries is as high as few hundred events per year for most of our models.

The uncertainties of population synthesis method (reflected on the predicted detection ranges) seem much reduced compared to the earlier results (see Fryer et al. 1999; Kalogera et al. 2001). This is related to the fact that in the present study we adopted a given set of single star evolution models (however note that we did explore the effects of varying wind mass-loss rates and helium-star evolution), and we have adopted a physically motivated initial-remnant mass relation based on hydrodynamical calculations of core-collapse events. In light of some indicative results from rotating star models (Heger, Langer

& Woosley 2000; Heger & Langer 2000), we can expect stellar evolution models to be updated in the future and we would regard this as progress in the field.

We regard the investigation of the physical properties of DCO as important as that of the rates and quite revealing in terms of their origin and robustness. The details have already been discussed earlier in the paper. From the point of view of gravitational-wave astrophysics, we hope these results will open new directions in anticipating and understanding properties of gravitational-wave sources. For example, distributions over components masses can be used to produce fake inspiral data to test the data analysis tools currently under development or evaluate detection efficiencies (we are currently involved in such an activity already planned within the LIGO Scientific Collaboration as part of the preparation for the LIGO I Scientific run in 2002). Predictions for physical properties can be used in developing specialized data-analysis tools to explore an astrophysically motivated parameter space, in cases where the unrestricted parameter space of inspiral signals is just far beyond any current or near-future computational capabilities (see Kalogera 2000). Looking a little more into the future, in the era when gravitational-wave astronomy is possible and physical properties are measurable, the identification of strong qualitative features (such as those discussed here: relative contributions of DCO classes, or presence or absence of certain peaks and other features) will allow us to evaluate some of the surviving theoretical models.

We thank Jarrod Hurley for many very useful comments on single star evolution, Teviet Creighton for discussions of LIGO project needs, Jeffrey McClintock for comments on the observed compact object mass distribution, Chris Fryer for his population synthesis and common-envelope insights, Ron Taam for his help in our common-envelope understanding, and Thomas Matheson for discussion of SN rates. KB acknowledges support from the Smithsonian Institution through a Predoctoral Fellowship, from the Lindheimer fund at Northwestern University, from the Polish Science Foundation (FNP) through a 2001 Polish Young Scientist Award, and from the Polish Nat. Res. Comm. (KBN) through grants 2P03D02219 and 5P03D01120. VK acknowledges support from the Smithsonian Institution through a Clay Fellowship and from NSF Grant PHY-0121420. TB acknowledges support from the Polish Nat. Res. Comm. (KBN) through grant 5P03D01120. VK and TB are also grateful for the hospitality and support of the Aspen Center for Physics.

APPENDIX

HYPER-CRITICAL ACCRETION ONTO COMPACT OBJECTS DURING COMMON ENVELOPE PHASE

Let us denote the mass of the compact object (NS or BH) by M_A , the mass of its companion (H-rich or He-rich giant) by M_B , its core mass by $M_{B,\text{core}}$, its radius by $R_{B,\text{ce}}$, and the binary semi-major axis by A_{ce} . Accretion onto the compact object can be initiated only once the binary separation becomes equal to the radius of the expanding giant donor. Both quantities have changed since the time of Roche-lobe filling to A_{acc} and $R_{B,\text{acc}}$, so that $A_{\text{acc}} = R_{B,\text{acc}}$. CE evolution and accretion onto the compact object will end when the giant's envelope has been ejected and the donor's mass changes from $M_{B,i}$ to $M_{B,f} = M_{B,\text{core}}$. Throughout the derivation α_{ce} is the CE efficiency parameter and λ is the numerical factor scaling the binding energy of the donor. The orbit is expected to be circular due to circularization on very short time scale as the donor approached Roche-lobe filling.

Following Bethe & Brown (1998) we write the energy loss rate related to the accretion onto the compact object

$$\dot{E}_{\text{acc}} = 0.5c_d G(M_B + M_A) A^{-1} \dot{M}_A \quad (\text{A1})$$

where c_d is the drag coefficient of the compact object with respect to the donor's envelope, and it is assumed $c_d = 6$ (Shima et al. 1985). The rate of orbital energy dissipation is given by:

$$-\dot{E}_{\text{orb}} = 0.5GM_B A^{-1} \dot{M}_A + 0.5GM_A A^{-1} \dot{M}_B - 0.5GM_A M_B A^{-2} \dot{A} \quad (\text{A2})$$

Orbital energy is dissipated due to the dynamical friction of accreting neutron star in the giant envelope. Thus, we may compare equations A.1 and A.2 ($\dot{E}_{\text{acc}} = -\dot{E}_{\text{orb}}$) and after taking derivative in respect to dM_B we obtain,

$$[c_d(M_B + M_A) - M_B] \frac{dM_A}{dM_B} = -M_A M_B A^{-1} \frac{dA}{dM_B} + M_A \quad (\text{A3})$$

During the phase of accretion we may express binding energy of donor envelope as,

$$-E_{\text{bind}} = GM_B(M_B - M_{B,\text{core}}) \lambda^{-1} A^{-1} \quad (\text{A4})$$

where instead of the donor radius we use the binary separation, which at the start of the accretion phase is equal to the donor radius ($A_{\text{acc}} = R_{B,\text{acc}}$). The rate of binding energy change can be written as,

$$-\dot{E}_{\text{bind}} = G\lambda^{-1} A^{-1} (2M_B - M_{B,\text{core}}) \dot{M}_B + GM_B \lambda^{-1} A^{-2} (M_{B,\text{core}} - M_B) \dot{A} \quad (\text{A5})$$

The donor envelope is ejected on the expense of the binary orbital energy, with an efficiency described by parameter α_{ce} . Thus, we write CE energy balance with respect to the donor mass as,

$$-\alpha_{\text{ce}} \left(-\frac{dE_{\text{orb}}}{dM_B} \right) = \left(-\frac{dE_{\text{bind}}}{dM_B} \right) \quad (\text{A6})$$

We use equations A.2, A.5, and A.6 to write:

$$M_B \frac{dM_A}{dM_B} = M_B A^{-1} [-2\lambda^{-1} \alpha_{\text{ce}}^{-1} (M_{B,\text{core}} - M_B) + M_A] \frac{dA}{dM_B} - 2\lambda^{-1} \alpha_{\text{ce}}^{-1} (2M_B - M_{B,\text{core}}) - M_A \quad (\text{A7})$$

We can next write out two ordinary differential equations to be solved:

$$\frac{dA}{dM_B} = \frac{M_A M_B h_1^{-1} + 2\lambda^{-1} \alpha_{\text{ce}}^{-1} (2M_B - M_{B,\text{core}}) + M_A}{M_A M_B^2 A^{-1} h_1^{-1} + M_B A^{-1} [-2\lambda^{-1} \alpha_{\text{ce}}^{-1} (M_{B,\text{core}} - M_B) + M_A]} \quad (\text{A8})$$

$$\frac{dM_A}{dM_B} = M_A h_1^{-1} (1 - M_B A^{-1} f_1(M_A, M_B, A)) \quad (\text{A9})$$

where $h_1 = c_d(M_B + M_A) - M_B$, and $f_1(M_A, M_B, A)$ is equal to the right hand side of equation (A.8). We know the initial and final values for M_B , the initial value for M_A , and we can calculate the initial value for A when accretion is initiated. To do so we use the CE energy balance for the pre-accretion period ($-\alpha_{\text{ce}} \Delta E_{\text{orb}} = \Delta E_{\text{bind}}$) and obtain:

$$A_{\text{acc}} = \frac{2(M_B - M_{B,\text{core}}) + \lambda \alpha_{\text{ce}} M_A}{2(M_B - M_{B,\text{core}}) R_B^{-1} + \lambda \alpha_{\text{ce}} M_A A_{\text{ce}}^{-1}} \quad (\text{A10})$$

where we set $R_{B,\text{acc}} = A_{\text{acc}}$. Equations A.8 and A.9 describe the accretion phase during CE evolution ($A < A_{\text{acc}}$), and we integrate them numerically from $M_{B,i}$ to $M_{B,\text{core}}$ to obtain the final binary separation and final mass of the accreting compact object.

REFERENCES

- Abramovici, A. et al. 1992, *Science*, 256, 325
- Abt, H. A. 1983, *ARA&A*, 21, 343
- Arzoumanian, Z., Cordes, J. M., & Chernoff, D. 1997, in "American Astronomical Society Meeting", 191, 11308
- Arzoumanian, Z., Cordes, J. M., & Wasserman, I. 1998, *ApJ*, 520, 696
- Avila-Rees, V. A. 1993, *Rev. Mex. Astron. Astrofis.*, 25, 79
- Bailyn, C. D., Jain, R. K., Coppi, P., & Orosz, J. A. 1998, *ApJ*, 499, 367
- Belczynski, K., & Bulik, T. 1999, *A&A*, 346, 91
- Belczynski, K., Bulik, T., & Zbijewski, W. 2000, *A&A*, 355, 479
- Belczynski, K., & Kalogera, V. 2001, *ApJ*, 550, L183
- Belczynski, K., Bulik, T., & Kalogera, V. 2002a, in preparation
- Belczynski, K., Bulik, T., & Kluzniak, W. 2002b, *ApJ*, accepted
- Belczynski, K., Bulik, T., & Rudak, B. 2002c, *ApJ*, 571, in press
- Bender, P. L. et al. 2000, *System and Technology Study Report*, ESA-SCI(2000)11; available at <ftp://ftp.rzg.mpg.de/pub/grav/lisa/sts-1.04.pdf>
- Bethe, H., & Brown, G. E. 1998, *ApJ*, 506, 780
- Bhattacharya, D., & van den Heuvel, E. P. J. 1991, *Phys. Rep.*, 203, 1
- Blitz, L. 1997, in "CO: Twenty-Five Years of Millimeter-Wave Spectroscopy", eds. W. B. Latter, et al. (Kluwer Academic Publishers), p. 11
- Blondin, J. M. 1986, *ApJ*, 308, 755
- Bloom, J. S., Sigurdsson, S., & Pols, O. R. 1999, *MNRAS*, 305, 763
- Branch, D., Livio, M., Yungelson, L. R., Boffi, F. R., & Baron, E. 1995, *PASP*, 107, 1019
- Brown, G. E. 1995, *ApJ*, 440, 270
- Brown, G. E., Lee, C. H., Wijers, R. A. M. J., Lee, H. K., Israelian, G., & Bethe, H. A. 2000, *New Astronomy*, 5, 191
- Brown, G. E., Weingartner, J. C., & Wijers, R. A. M. J. 1996, *ApJ*, 463, 297
- Cappellaro, E., Evans, R., & Turatto, M. 1999, *A&A*, 351, 459
- Cappellaro, E., Turatto, M., Benetti, S., Tsvetkov, D. Y., Bartunov, O. S., & Makarova, I. N. 1993a, *A&A*, 268, 472
- Cappellaro, E., Turatto, M., Benetti, S., Tsvetkov, D. Y., Bartunov, O. S., & Makarova, I. N. 1993b, *A&A*, 273, 383
- Caron, B. et al. 1995, in *Gravitational Wave Experiments*, eds. E. Coccia, G. Pizzella, & F. Ronga, World Scientific, Singapore
- Chevalier, R. A. 1989, *ApJ*, 346, 847
- Chevalier, R. A. 1993, *ApJ*, 411, L33
- Cordes, J., & Chernoff, D. F. 1998, *ApJ*, 505, 315
- Curran, S. J., & Lorimer, D. R. 1995, *MNRAS*, 276, 347
- Danzmann, K. et al. 1995, in *Gravitational Wave Experiments*, eds. E. Coccia, G. Pizzella, & F. Ronga, World Scientific, Singapore
- De Doner, E., & Vanbeveren, D. 1998, *A&A*, 333, 557
- Delgado, A. J., & Thomas, H. C. 1981, *A&A*, 96, 142
- Dewi, J. D. M., & Tauris, T. M. 2000, *A&A*, 360, 1043
- Duquennoy, A., & Mayor, M. 1991, *A&A*, 248, 485
- de Kool, M. 1990, *ApJ*, 358, 189
- Froning, C. S., & Robinson, E. L. 2001, *ApJ*, submitted [astro-ph/0101421]
- Eggleton, P. P. 1971, *MNRAS*, 151, 351
- Eggleton, P. P. 1972, *MNRAS*, 156, 361
- Eggleton, P. P. 1973, *MNRAS*, 163, 279
- Einstein, A. 1916, *Preuss. Akad. Wiss. Berlin, Sitzungsberichte der physikalisch-mathematischen Klasse*, 688
- Einstein, A. 1918, *Preuss. Akad. Wiss. Berlin, Sitzungsberichte der physikalisch-mathematischen Klasse*, 154
- Ergma, E., & van den Heuvel, E. P. J. 1998, *A&A*, 331, L29
- Fryer, C. L. 1999, *ApJ*, 522, 413
- Fryer, C. L., & Kalogera, V. 1997, *ApJ*, 489, 244
- Fryer, C. L., & Kalogera, V. 2001, *ApJ*, 554, 548
- Fryer, C. L., Woosley, S. E., & Hartmann, D. H. 1999, *ApJ*, 526, 152
- Gilmore, G. 2001, to appear in "Galaxy Disks and Disk Galaxies", eds. J. G. Funes & E. M. Corsini, San Francisco, ASP
- Habets, G. M. H. J. 1987, *A&AS*, 69, 183
- Hamann, W. R., Koesterke, L., & Wessolowski, U. 1995, *A&A*, 299, 151
- Han, Z., Podsiadlowski, P., & Eggleton, P. P. 1994, *MNRAS*, 270, 121
- Hartman, J. W. 1997, *A&A*, 322, 127
- Heger, A., & Langer, N. 2000, *ApJ*, 544, 1016
- Heger, A., Langer, N., & Woosley, S. E. 2000, *ApJ*, 528, 368
- Heggie, D. C. 1975, *MNRAS*, 173, 729
- Hjellming, M. S., & Webbink, R. F. 1987, *ApJ*, 318, 794
- Hulse, R. A., & Taylor, J. H. 1974, *ApJ*, 191, L59
- Hulse, R. A., & Taylor, J. H. 1975a, *ApJ*, 195, L51
- Hulse, R. A., & Taylor, J. H. 1975b, *ApJ*, 201, L55
- Humphreys, R. M., & Davidson, K. 1994, *PASP*, 106, 1025
- Hurley, J. R., Pols, O. R., & Tout, C. A. 2000, *MNRAS*, 315, 543
- Iben, I., & Livio, M. 1993, *PASP*, 105, 1373
- Junker, W., & Schaefer, G. 1992, *MNRAS*, 254, 146
- Kalogera, V. 1996, *ApJ*, 471, 352
- Kalogera, V. 2000, in *Gravitational Waves*, Third Edoardo Amaldi Conference, ed. S. Meshkov, AIP Conference Proceedings, Vol. 523, New York: AIP Press, p.41
- Kalogera, V., & Belczynski, K. 2001, in *Astrophysical Sources for Ground-based Gravitational Wave Detectors*, ed. J. M. Centrella, AIP Conference Proceedings, Vol. 575, New York: AIP Press, p.107
- Kalogera, V., Narayan, R., Spergel, D. N., & Taylor, J. H. 2001, *ApJ*, accepted [astro-ph/0012038]
- Kalogera, V., & Webbink, R. F. 1996, *ApJ*, 458, 301
- Kauffmann, G., Charlot, S., & Balogh, M. L. 2001, *MNRAS*, submitted [astro-ph/0103130]
- Kim, C., Kalogera, V., & Lorimer, D. R. 2001, in preparation
- Kroupa, P., Tout, C. A., & Gilmore, G. 1993, *MNRAS*, 262, 545
- Kudritzki, R. P., Pauldarch, A., Puls, J., & Abbot, D. C. 1989, *A&A*, 219, 205
- Kudritzki, R. P., & Reimers, D. 1978, *A&A*, 70, 227
- Kuiper, G. P. 1935, *PASP*, 47, 15
- Lacey, C. G., & Fall, S. M. 1985, *ApJ*, 290, 154
- Liebendoerfer, M. et al. 2001, *Phys. Rev. D*, 63, 103004
- Lipunov, V. M., Postnov, K. A., & Prokhorov, M. E. 1997, *MNRAS*, 288, 245
- McClintock, J. E., Garcia, M. R., Caldwell, N., Falco, E. E., Garnavich, P. M., & Zhao, P. 2001, *ApJ*, submitted [astro-ph/0101421]
- Narayan, R., Piran, T., Shemi, A. 1991, *ApJ*, 379, L17
- Nelemans, G., Yungelson, L. R., Portegies Zwart, S. F., & Verbunt, F. 2001a, *A&A*, 365, 491
- Nelemans, G., Yungelson, L. R., & Portegies Zwart, S. F. 2001b, *A&A*, 375, 890
- Nieuwenhuijzen, H., & de Jager, C. 1990, *A&A*, 231, 134
- Orosz, J. A. et al. 2001, *ApJ*, submitted [astro-ph/0103045]
- Ostriker, J. P. 1975, paper presented at IAU Symp. 73, The Structure and Evolution of Close Binary Systems
- Paczynski, B. 1976, in *The Structure and Evolution of Close Binary Systems*, ed. P. Eggleton, S. Milton, & J. Whelan (Dordrecht, Reidel), p. 75
- Paczynski, B. 1990, *ApJ*, 348, 485
- Perna, R., & Belczynski, K. 2002, *ApJ*, 570, in press
- Peters, P. C. 1964, *Phys. Rev.*, 136, B1224
- Phinney, E. S. 1991, *ApJ*, 380, L17
- Podsiadlowski, P., Joss, P. C., & Hsu, J. J. L. 1992, *ApJ*, 391, 246
- Podsiadlowski, P., Nomoto, K., Maeda, K., Nakamura, T., Mazzali, P., & Schmidt, B. 2001, *ApJ*, submitted [astro-ph/0109244]
- Pols, O. R., Tout, C. A., Eggleton, P. P., & Han, Z. 1995, *MNRAS*, 274, 964
- Pols, O. R., Schroder, K. P., Hurley, J. R., Tout, C. A., & Eggleton, P. P. 1998, *MNRAS*, 298, 525
- Portegies Zwart, S. F., & Verbunt, F. 1996, *A&A*, 309, 179
- Portegies Zwart, S. F., & Yungelson, L. R. 1998, *A&A*, 332, 173
- Rasio, F. A., & Livio, M. 1996, *ApJ*, 471, 366
- Ritter, H. 1999, *MNRAS*, 309, 360
- Salpeter, E. E. 1955, *ApJ*, 121, 161
- Sandeman, R. J. 1998, in *Second Workshop on Gravitational Wave Data Analysis*, eds. M. Davies, & P. Hello, Editions Frontieres, Paris
- Scalo, J. M. 1986, *Fundam. Cosmic Phys.*, 11, 1
- Schaller, G., Schaerer, D., Meynet, G., & Maeder, A. 1992, *A&AS*, 269, 331
- Tagoshi, H. et al. 2001, *Phys. Rev.*, 63, 231
- Taam, R. E. 1996, in *Compact Stars in Binaries*, eds. J. van Paradijs et al., pp. 3
- Taam, R. E., & Sandquist, E. L. 2000, *ARA&A*, 38, 113
- Taylor, J. H., & Weisberg, J. M. 1982, *ApJ*, 253, 908
- Taylor, J. H., & Weisberg, J. M. 1989, *ApJ*, 345, 434
- Thorne, K. S. 1987, in *300 Years of Gravitation*, eds. S. W. Hawking & W. Israel, Cambridge U. Press, Cambridge, UK
- Thorsett, S. E., & Chakrabarty, D. 1999, *ApJ*, 512, 288
- Tutukov, A. V., & Yungelson, L. 1993, *Astron. Rep.*, 37, 411
- Vanbeveren, D., Van Rensbergen, W., & De Loore, C. 1998, in "The Brightest Binaries", *Astrophysics and Space Science Library*, Vol. 232, p. 124
- van den Heuvel, E. P. J. 1992, in *X-Ray Binaries and Recycled Pulsars*, eds. E. P. J. van den Heuvel & S. A. Rappaport, pp. 233
- van der Kruit, P. C. 1987, in "The Galaxy", eds. G. Gilmore & B. Carswell, Dordrecht: Reidel, p. 27
- Vassiliadis, E., & Wood, P. R. 1993, *ApJ*, 413, 641
- Verbunt, F., & Van den Heuvel, E. P. J. 1995, in "X-ray Binaries", eds. W. H. G. Lewin, J. van Paradijs & E. P. J. Van den Heuvel, Cambridge Astrophysics Series, Vol. 26, p. 457
- Wagner, R. M., Foltz, C. B., Shahbaz, T., Casares, J., Charles, P. A., Starrfield, S. G., & Hewett, P. 2001, *ApJ*, 556, in press [astro-ph/0104032]

- Webbink, R. F. 1984, ApJ, 277, 355
Wellstein, S., & Langer, N. 1999, A&A, 350, 148
Woosley, S.E. 1986, in "Nucleosynthesis and Chemical Evolution",
16th Saas-Fee Course, eds. B. Hauck et al., Geneva Obs., p. 1
Woosley, S.E., Langer, N., Weaver, T.A. 1995, ApJ, 448, 315
Zahn, J. R. 1978, A&A, 67, 162

TABLE 1
POPULATION SYNTHESIS MODEL ASSUMPTIONS

Model	Description
A	standard model described in § 2.1 and § 2.2
B1–13	zero kicks, single Maxwellian with $\sigma = 10, 20, 30, 40, 50, 100, 200, 300, 400, 500, 600 \text{ km s}^{-1}$, “Paczynski” kicks with $\sigma = 600 \text{ km s}^{-1}$
C	no hyper-critical accretion onto NS/BH in CEs
D1–2	maximum NS mass: $M_{\text{max,NS}} = 2, 1.5 M_{\odot}$
E1–3	$\alpha_{\text{CE}} \times \lambda = 0.1, 0.5, 2$
F1–2	mass fraction accreted: $f_{\text{a}} = 0.1, 1$
G1–2	wind changed by $f_{\text{wind}} = 0.5, 2$
H1–2	Convective Helium giants: $M_{\text{conv}} = 4.0, 0 M_{\odot}$
I	burst-like star formation history
J	primary mass: $\propto M_1^{-2.35}$
K1–2	binary fraction: $f_{\text{bi}} = 0.25, 0.75$
L1–2	angular momentum of material lost in MT: $j = 0.5, 2.0$
M1–2	initial mass ratio distribution: $\Phi(q) \propto q^{-2.7}, q^3$
N	no helium giant radial evolution
O	partial fall back for $5.0 < M_{\text{CO}} < 14.0 M_{\odot}$

TABLE 2
POPULATION SYNTHESIS ACCURACY

Coalescing Population	Mean Rate ^a	Max Change in Rate ^a	Mean Number
NS-NS	52.7 \pm 1.1 (2%)	4.4 (8%)	1754
BH-NS	8.1 \pm 0.6 (7%)	2.2 (27%)	269
BH-BH	25.6 \pm 0.8 (3%)	3.9 (15%)	852
Total	86.3 \pm 1.2 (1%)	5.5 (6%)	2875

^aGalactic Coalescence Rate (Myr^{-1}).

TABLE 3
DOUBLE COMPACT OBJECT FORMATION CHANNELS - STANDARD MODEL

Formation Channel	Relative Efficiency ^a	Evolutionary History ^b
NSNS:01	20.3 %	NC:a→b, SN:a, HCE:b→a, HCE:b→a, SN:b
NSNS:02	10.8 %	NC:a→b, SCE:b→a, NC:a→b, SN:a, HCE:b→a, SN:b
NSNS:03	5.5 %	SCE:a→b, SN:a, HCE:b→a, HCE:b→a, SN:b
NSNS:04	4.0 %	NC:a→b, SCE:b→a, SCE:b→a, SN:b, HCE:a→b, SN:a
NSNS:05	3.2 %	DCE:a→b, SCE:a→b, SN:a, HCE:b→a, SN:b
NSNS:06	2.5 %	SCE:a→b, SCE:b→a, NC:a→b, SN:a, HCE:b→a, SN:b
NSNS:07	2.2 %	NC:a→b, NC:a→b, SN:a, HCE:b→a, HCE:b→a, SN:b
NSNS:08	2.0 %	NC:a→b, DCE:b→a, SN:a, HCE:b→a, SN:b
NSNS:09	2.0 %	DCE:a→b, DCE:a→b, SN:a, SN:b
NSNS:10	1.6 %	NC:a→b, SCE:b→a, SN:b, HCE:a→b, SN:a
NSNS:11	1.5 %	NC:a→b, SCE:b→a, DCE:b→a, SN:a, SN:b
NSNS:12	1.5 %	NC:a→b, SCE:b→a, DCE:a→b, SN:a, SN:b
NSNS:13	1.0 %	DCE:a→b, SN:a, HCE:b→a, SN:b
NSNS:14	3.0 %	all other
BHNS:01	4.5 %	NC:a→b, SN:a, HCE:b→a, SN:b
BHNS:02	1.6 %	NC:a→b, SCE:b→a, SN:a, SN:b
BHNS:03	1.3 %	SCE:a→b, SN:a, HCE:b→a, NC:b→a, SN:b
BHNS:04	2.0 %	all other
BHBH:01	17.7 %	NC:a→b, SN:a, HCE:b→a, SN:b
BHBH:02	10.5 %	NC:a→b, SCE:b→a, SN:a, SN:b
BHBH:03	1.4 %	all other

^aNormalized to the total DCO population.

^bSequences of different evolutionary phases for the primary (a) and the secondary (b): non-conservative MT (NC), single common envelope (SCE), double common envelope (DCE), common envelope with hyper-critical accretion (HCE), supernova explosion/core-collapse event (SN). Arrows mark direction of MT episodes.

TABLE 4
GALACTIC DOUBLE COMPACT OBJECT COALESCENCE RATES
(Myr⁻¹)

Model ^a	NS-NS	BH-NS	BH-BH	Total
A	52.7	8.1	25.6	86.3
B1	292.4	18.2	32.7	343.2
B2	299.6	19.4	31.8	350.8
B3	302.2	19.6	34.2	356.0
B4	285.2	19.1	34.2	338.5
B5	251.0	19.5	34.3	304.7
B6	226.8	16.4	34.1	277.3
B7	128.1	14.6	30.7	173.3
B8	57.5	10.1	29.2	96.8
B9	33.2	5.7	23.2	62.1
B10	18.2	3.7	21.0	42.9
B11	12.0	2.1	18.1	32.2
B12	8.0	1.6	15.1	24.6
B13	91.0	10.3	27.3	128.6
C	43.2	5.6	23.2	72.1
D1	33.6	23.3	31.1	88.0
D2	9.1	36.2	42.2	87.5
E1	2.7	4.8	5.6	13.1
E2	23.5	6.3	23.1	53.0
E3	109.0	8.7	11.5	129.2
F1	22.1	9.3	8.7	40.1
F2	54.3	8.6	7.2	70.1
G1	43.9	14.2	75.6	133.7
G2	92.2	1.3	0.0	93.5
H1	37.9	7.8	26.6	72.3
H2	0.9	6.0	26.3	33.2
I	54.5	10.0	33.6	98.1
J	58.1	12.8	41.9	112.8
K1	22.5	3.4	10.4	36.2
K2	90.2	13.5	41.6	145.4
L1	78.9	9.2	10.0	98.1
L2	12.0	6.2	10.5	28.7
M1	6.2	4.0	5.8	16.0
M2	114.2	8.4	31.5	154.1
N	34.4	10.7	24.5	69.6
O	51.9	5.7	4.0	61.6

^afor definition of models see Table 1

TABLE 5
NS-NS EMPIRICAL COALESCENCE RATE CORRECTION FACTORS

Model ^a	Group I all	Group II $t_{\text{merg}} < 1 \text{ Myr}$	Group III $t_{\text{merg}} < 1 \text{ Myr}$	Total Rate	Empirical Rate Correction Factor
A	4.4	26.9	0.1	52.7	2.5
B1	6.0	146.7	0.0	292.4	2.1
B6	6.5	121.6	0.0	226.8	2.3
B7	5.2	68.0	0.1	128.1	2.3
B8	4.7	27.6	0.2	57.5	2.3
B9	4.3	17.0	0.1	33.2	2.8
B10	2.8	8.8	0.1	18.2	2.8
B11	2.2	6.1	0.0	12.0	3.3
B12	1.9	4.2	0.0	8.0	4.2
B13	4.6	48.4	0.1	91.0	2.4
C	3.2	22.1	0.2	43.2	2.4
D1	4.9	15.1	0.0	33.6	2.5
D2	3.6	2.8	0.0	9.1	3.3
E1	0.4	1.9	0.0	2.5	6.1
E2	3.1	15.1	0.1	23.5	4.5
E3	5.2	28.0	0.2	109.0	1.4
F1	2.3	12.2	0.1	22.1	2.9
F2	2.3	16.1	0.8	54.3	1.5
G1	3.3	23.7	0.1	43.9	2.6
G2	7.3	38.0	0.2	92.2	2.0
H1	3.3	20.9	0.0	37.9	2.8
H2	0.0	0.0	0.1	0.9	1.1
I	4.0	28.5	0.0	54.5	2.5
J	4.4	29.4	0.1	58.1	2.4
K1	1.8	11.2	0.1	22.5	2.5
K2	7.4	44.9	0.2	90.2	2.5
L1	6.3	32.7	1.1	78.9	2.0
L2	2.0	5.6	0.1	12.0	2.8
M1	0.2	3.9	0.0	6.2	3.0
M2	14.0	51.6	0.2	114.2	2.4
N	0.0	0.0	1.1	34.4	1.0
O	4.3	26.5	0.1	51.9	2.5

^afor definition of models see Table 1

TABLE 6
PREDICTED LIGO I DETECTION RATES (yr^{-1})

Binary Type	Standard Model	Range (all models)
NS-NS	1×10^{-2}	$2 \times 10^{-4} - 7 \times 10^{-1}$
BH-NS	2×10^{-2}	$2 \times 10^{-3} - 7 \times 10^{-2}$
BH-BH	8×10^{-1}	0 – 2
Total	8×10^{-1}	$2 \times 10^{-3} - 2$

TABLE 7
PREDICTED LIGO II DETECTION RATES (yr^{-1})

Binary Type	Standard Model	Range (all models)
NS-NS	6×10^1	$1 - 4 \times 10^2$
BH-NS	8×10^1	$9 - 4 \times 10^2$
BH-BH	2×10^3	$0 - 8 \times 10^3$
Total	3×10^3	$1 \times 10^1 - 8 \times 10^3$

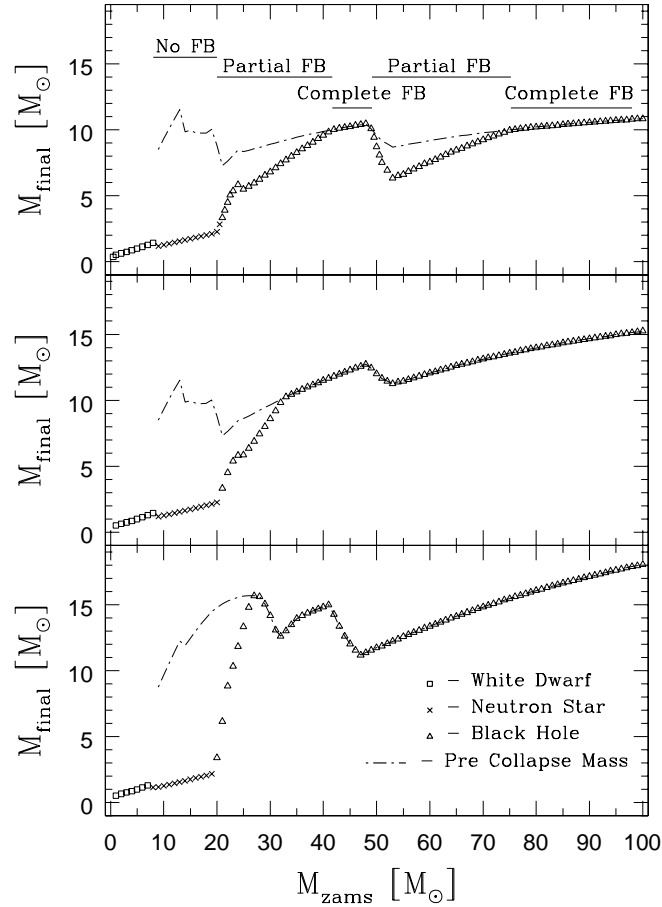


Fig. 1.— Final remnant masses shown as a function of progenitor ZAMS mass, for single Population I stars ($Z = 0.02$) and for three different wind mass-loss rates. Top panel: standard HPT wind mass-loss rate. Middle panel: Wolf-Rayet wind rates decreased by two. Bottom panel: all wind mass-loss rates decreased by a factor of two. Different symbols represent different remnant types (square: white dwarf; cross: neutron star; triangle: black hole). Stellar masses just prior to the collapse are shown by the dot-dashed line. In the top panel, we also mark the ranges of initial masses, for which NS or BH are formed without any fall back, and with partial or complete fall back in core-collapse events of massive stars. In all panels, a maximum NS mass of $3 M_{\odot}$ has been assumed. Masses of WD remnants are calculated as in HPT.

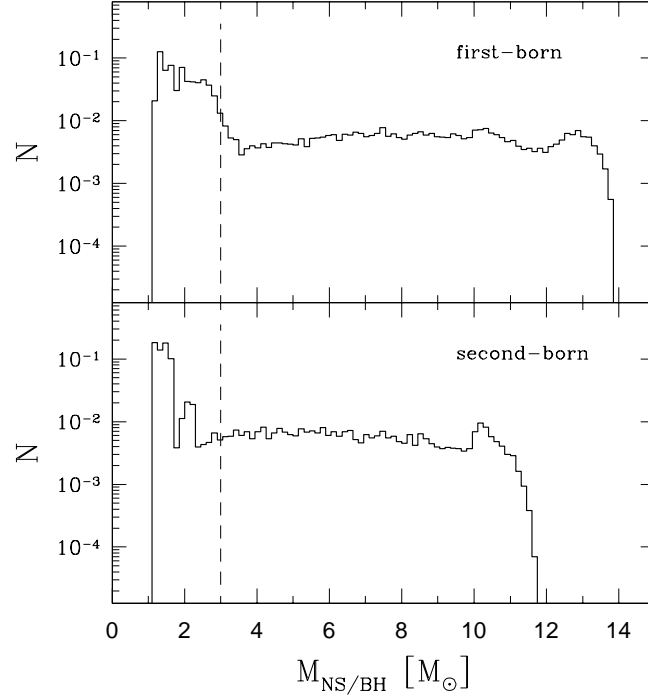


Fig. 2.— Normalized distributions of the compact object masses in coalescing NS-NS, BH-NS and BH-BH systems for the standard model. We show the mass distributions for first- and second-born compact objects in the top and bottom panel, respectively. The distributions are calculated using a total number of 28655 coalescing DCO formed out of 10^7 primordial binaries. Note that the standard model choice of the maximum NS mass is: $M_{\text{max}}^{\text{NS}} = 3 M_{\odot}$ (marked with the dashed line).

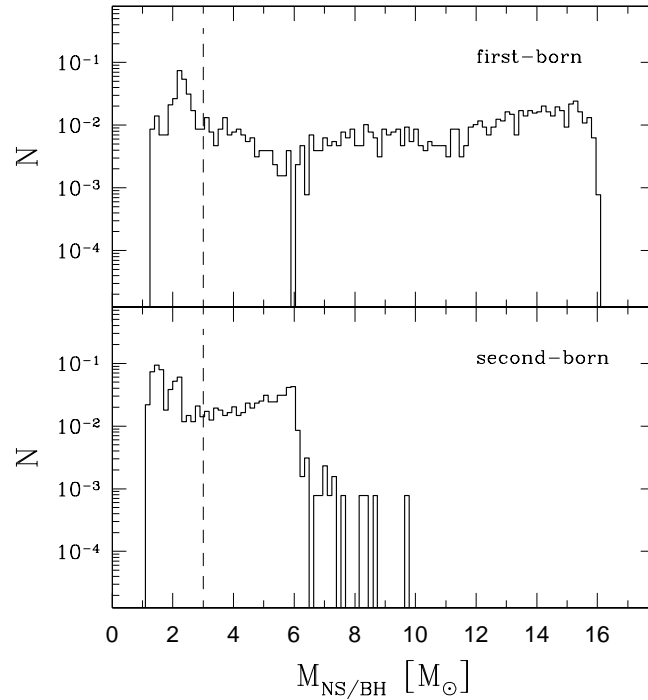


Fig. 3.— Normalized distributions of the compact object masses in coalescing NS-NS, BH-NS and BH-BH systems for model E1 with very low CE efficiency: $\alpha_{\text{CE}} \times \lambda = 0.1$. We show the mass distributions for first- and second-born compact objects in the top and bottom panel, respectively. The distributions are calculated using a total number of 1283 coalescing DCO formed out of 3×10^6 primordial binaries. This case of very low CE efficiency results in very low DCO rates and relatively small-number statistics. Note that the standard model choice of the maximum NS mass is: $M_{\text{max}}^{\text{NS}} = 3 M_{\odot}$ (marked with the dashed line).

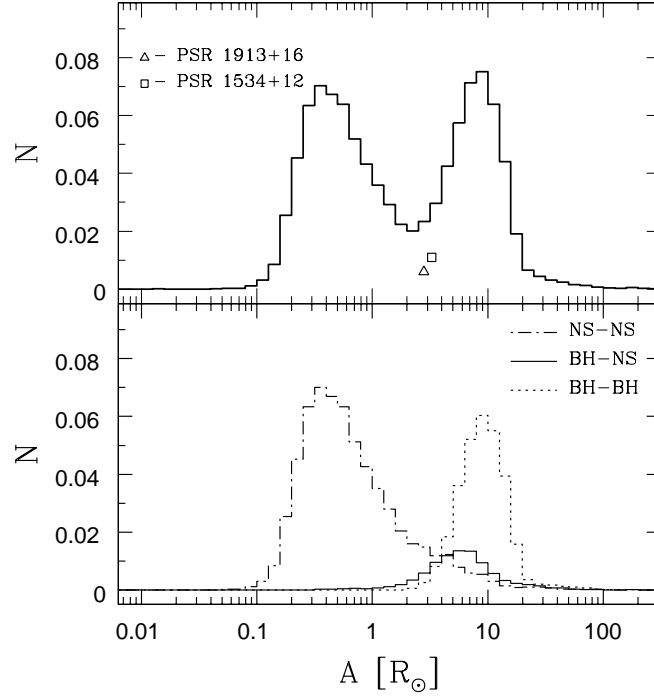


Fig. 4.— Normalized distributions of orbital separations of coalescing DCO at the time of their formation, for our standard model, for all DCO (top) and for the three classes separately (bottom). For comparison, we also show the observed orbital separations of the 2 coalescing NS-NS systems found in the Galactic field, PSR 1913+16 and PSR 1534+12.

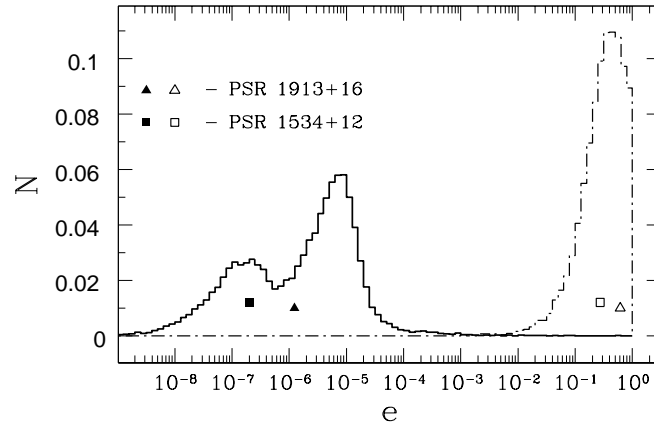


Fig. 5.— Normalized eccentricity distributions of coalescing DCO for our standard model at the time of their formation (dot-dashed line) and at the time the orbit decayed so that the corresponding gravitational-wave frequency is about 40 Hz, i.e., the system is entering the LIGO I band (solid line). For comparison we also show the two observed short-period NS-NS systems: their current (open symbols) eccentricities and the eccentricities as they enter the LIGO I band (filled symbols).

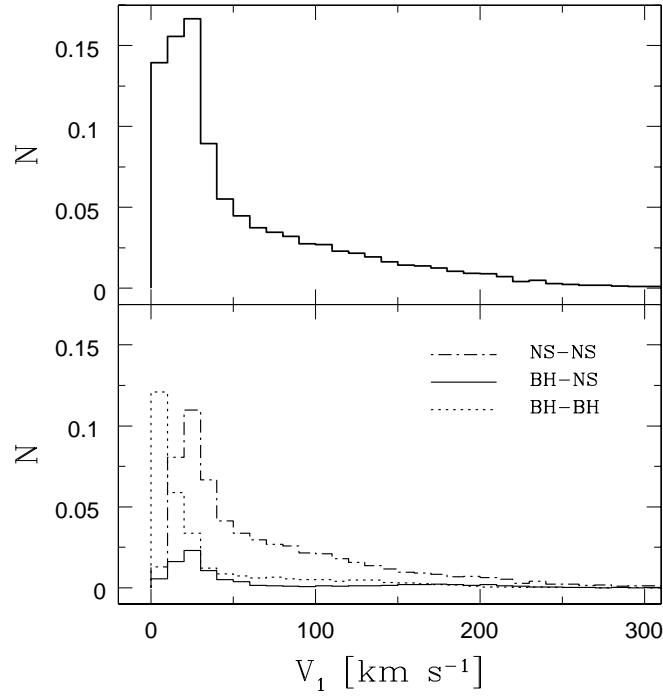


Fig. 6.— Normalized distributions of DCO systemic velocities acquired after the first core-collapse event, for our standard model, for the whole population (top) and for each DCO class separately (bottom).

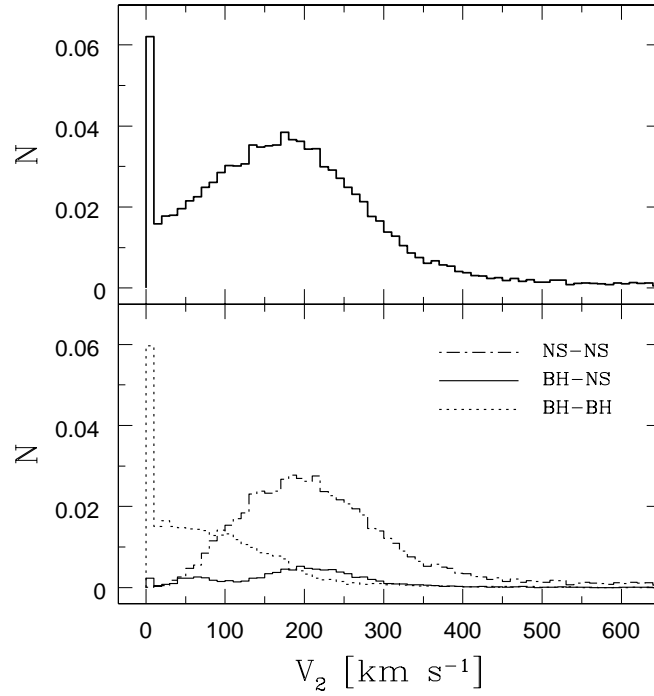


Fig. 7.— Normalized distributions of DCO systemic velocities acquired after the second core-collapse event, for our standard model, for the whole population (top) and for each DCO class separately (bottom).

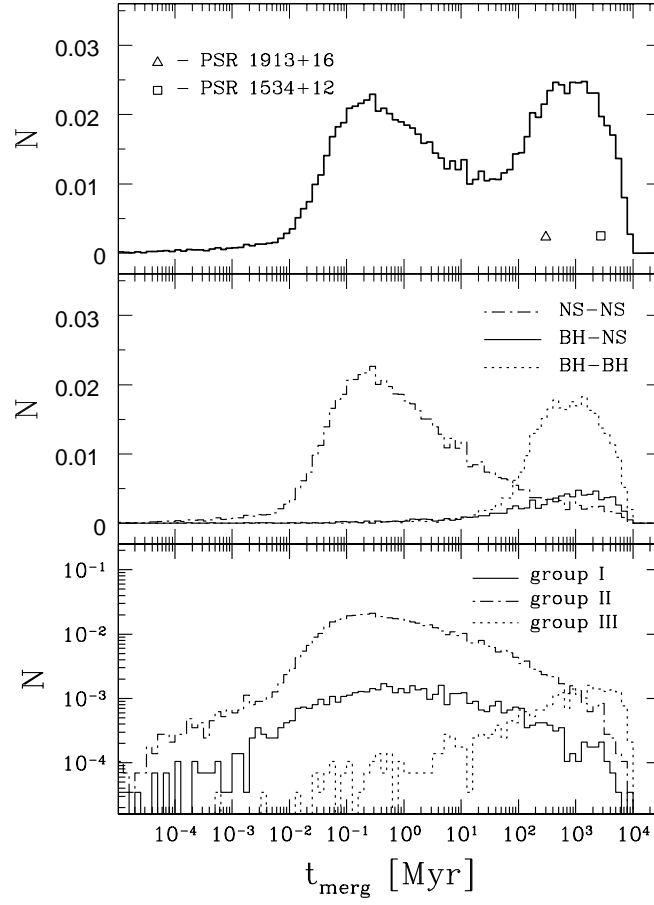


Fig. 8.— Normalized merger time distributions shown for our standard model, for the whole DCO population (top), for each of the DCO classes (middle), and for each of the three major NS-NS groups (bottom). The merger of the two observed systems are also shown in the top panel.

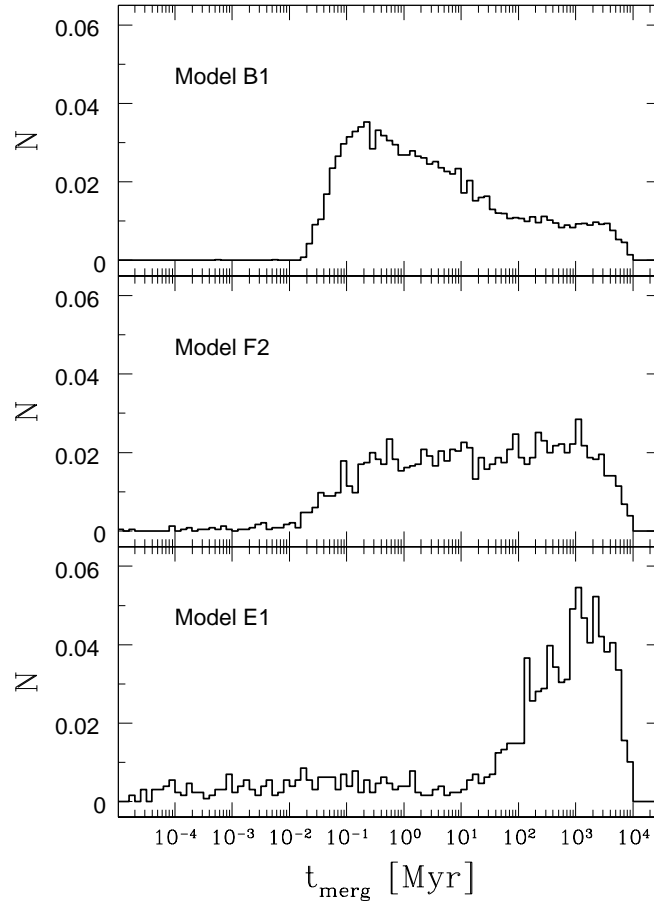


Fig. 9.— Normalized merger time distributions of coalescing DCO for models B1 (top panel), F2 (middle panel) and E1 (bottom panel). The distributions are normalized to the total number of coalescing DCO: 10841, 2352, 1283 for models B1, F2 and E1, respectively; formed out of 10^6 primordial binaries for model B1 and F2, and out of 3×10^6 binaries for model E1.

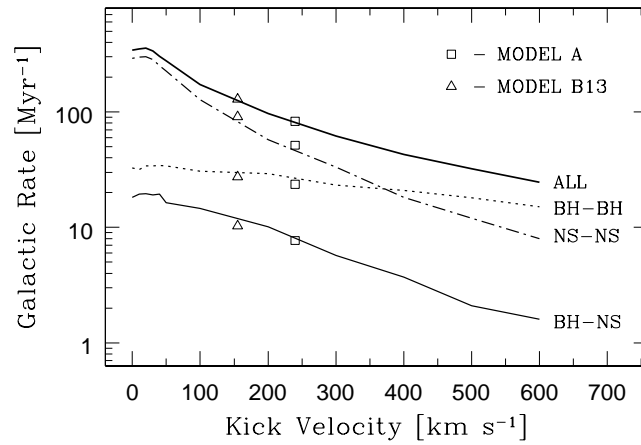


Fig. 10.— Dependence of Galactic coalescence rates on the assumed natal kick velocity distribution. Lines connect rates for models B1-B12 and the horizontal scale shows the width of Maxwellian kick distribution of a given model. Points mark rates for our standard model (A) and model with “Paczynski-like” kick distribution (B13). The horizontal position for these two models does not correspond to the horizontal axis scale, but instead is chosen so that the predicted rates approximately match the curve for the Maxwellian kick distributions.